Precise Orbit Determination

Adrian Jäggi

Astronomical Institute
University of Bern

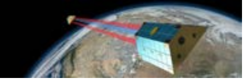

Lecture Contents

1. Introduction
2. Global Positioning System
3. Different Orbit Representations
4. Principles of Orbit Determination
5. GPS-based LEO POD
6. Orbit Validation

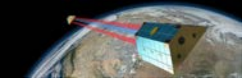

A multitude of Earth Observation Satellites

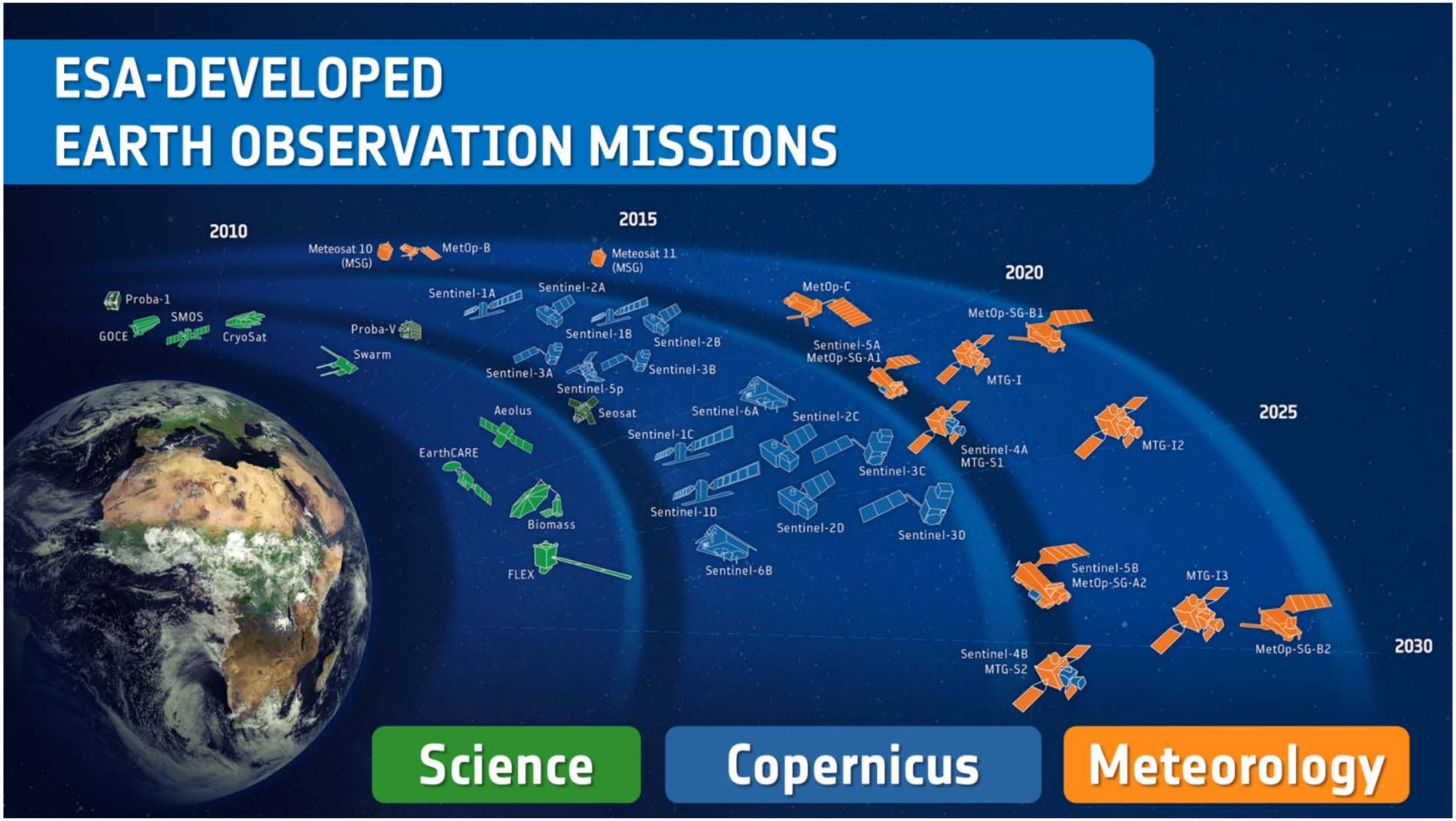
ESA-DEVELOPED
EARTH OBSERVATION MISSIONS
2010
2015
2020
2025
2030
Proba-1
SMOS
GOCE
CryoSat
Meteosat 10 (MSG)
MetOp-B
Proba-V
Swarm
Sentinel-1A
Sentinel-2A
Meteosat 11 (MSG)
Sentinel-1B
Sentinel-2B
Sentinel-3A
Sentinel-3B
Sentinel-5p
Aeolus
Seosat
EarthCARE
Biomass
FLEX
Sentinel-6A
Sentinel-1C
Sentinel-1D
Sentinel-6B
Sentinel-2C
Sentinel-2D
Sentinel-3C
Sentinel-3D
MetOp-C
Sentinel-5A
MetOp-SG-A1
MetOp-SG-B1
MTG-I
Sentinel-4A
MTG-S1
MTG-I2
Sentinel-5B
MetOp-SG-A2
MTG-I3
MetOp-SG-B2
Sentinel-4B
MTG-S2
Science
Copernicus
Meteorology

Precise Tracking Data in Near Earth Space

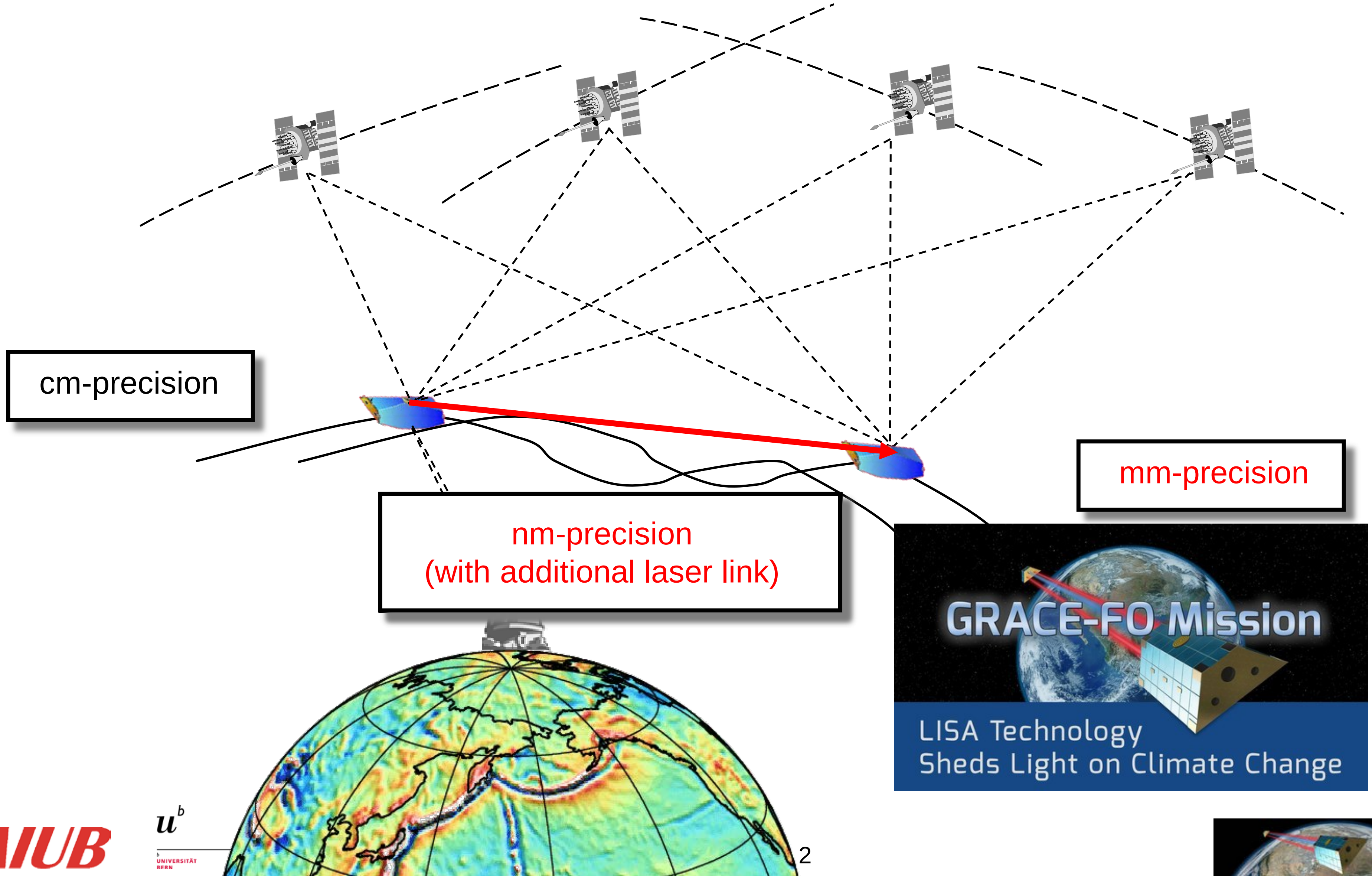

cm-precision

mm-precision

nm-precision
(with additional laser link)

GRACE-FO Mission
LISA Technology
Sheds Light on Climate Change

Low Earth Orbiters (LEOs)

CHAMP

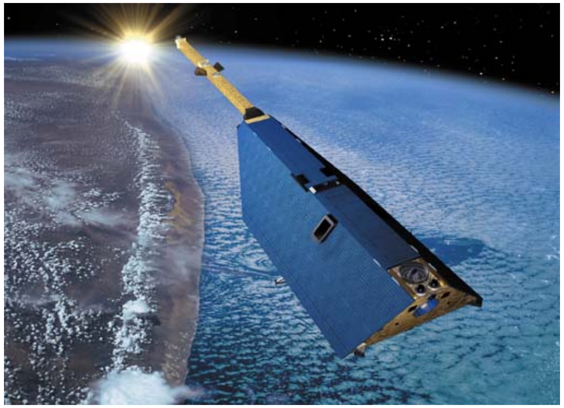

CHAllenging **M**inisatellite **P**ayload

GRACE

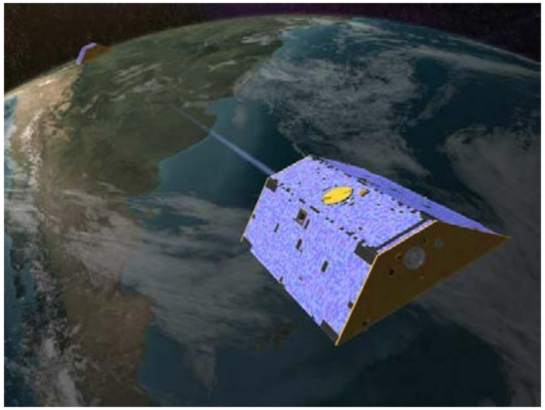

Gravity **R**ecovery **A**nd **C**limate **E**xperiment

GOCE

Gravity and steady-state **O**cean **C**irculation **E**xplorer

Of course, there are many more missions equipped with GPS receivers

Jason

Jason-2

MetOp-A

Icesat

COSMIC

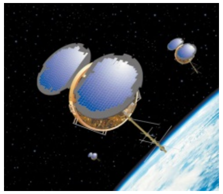

LEO Constellations

TanDEM-X

Swarm

Sentinel

GRACE-FO

GRACE-FO Mission
LISA Technology
Sheds Light on Climate Change

COSMIC-2

LEO CubeSats

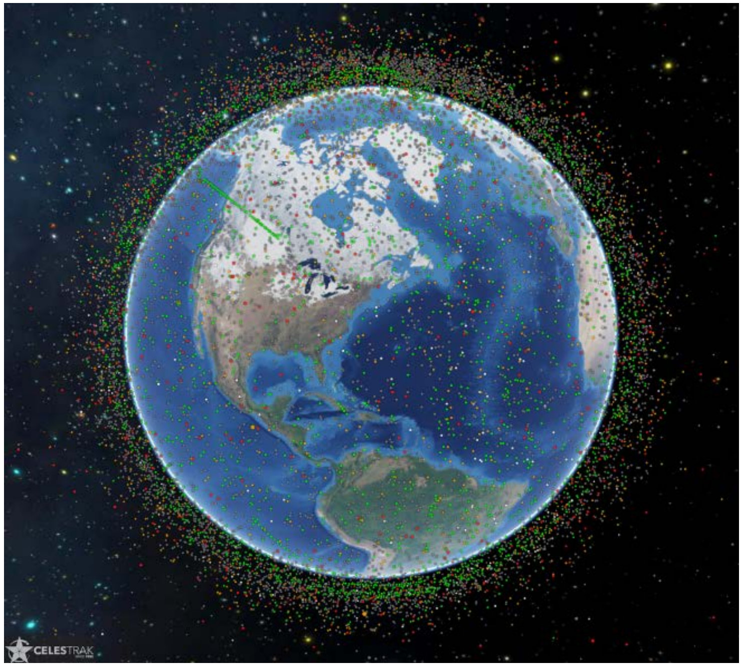

A multitude of **CubeSats** already exist or are planned for the future

e.g.

Spire

~ 100 Spire satellites are already in different orbits, offering dual-frequency high-quality GPS data

Many more will follow …

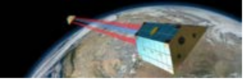

Global Positioning System

Introduction to GPS

GPS

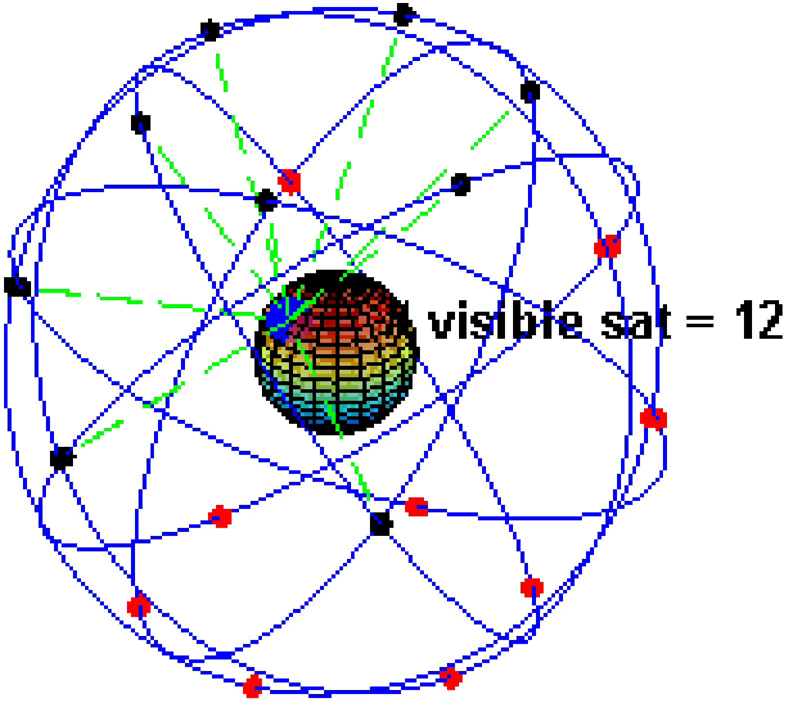
visible sat = 12

Galileo

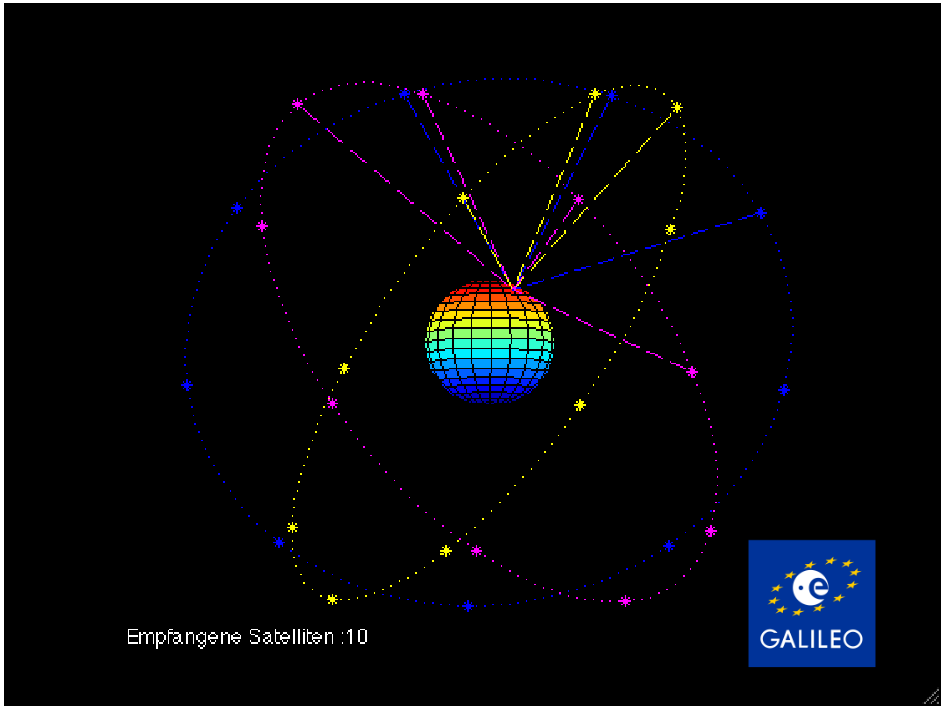
Empfangene Satelliten :10
GALILEO

Other **Global Navigation Satellite Systems** (GNSS) are also available (GLONASS, Galileo, Beidou), but for a long time no multi-GNSS spaceborne receivers were in orbit. This changed with the launches of Fengyun-3, COSMIC-2, Sentinel-6.

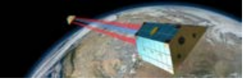

Introduction to GPS

GPS: **G**lobal **P**ositioning **S**ystem

Characteristics:

- Satellite system for (real-time) **Positioning** and **Navigation**
- **Global** (everywhere on Earth, up to altitudes of 5000km) and **at any time**
- **Unlimited** number of users
- **Weather-independent** (radio signals are passing through the atmosphere)
- **3-dimensional position**, **velocity** and **time** information

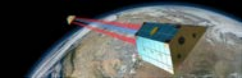

GPS Segments

The GPS consists of **3 main segments**:

- **Space Segment**: the satellites and the constellation of satellites
- **Control Segment**: the ground stations, infrastructure and software for operation and monitoring of the GPS
- **User Segment**: all GPS receivers worldwide and the corresponding processing software

We should add an important **4th segment**:

- **Ground Segment**: all civilian permanent networks of reference sites and the international/regional/local services delivering products for the users

Space Segment

- The space segment nominally consists of **24 satellites**, presently: 31 active GPS satellites
- Constellation design: at least **4 satellites** in view from **any location** on the Earth at **any time**

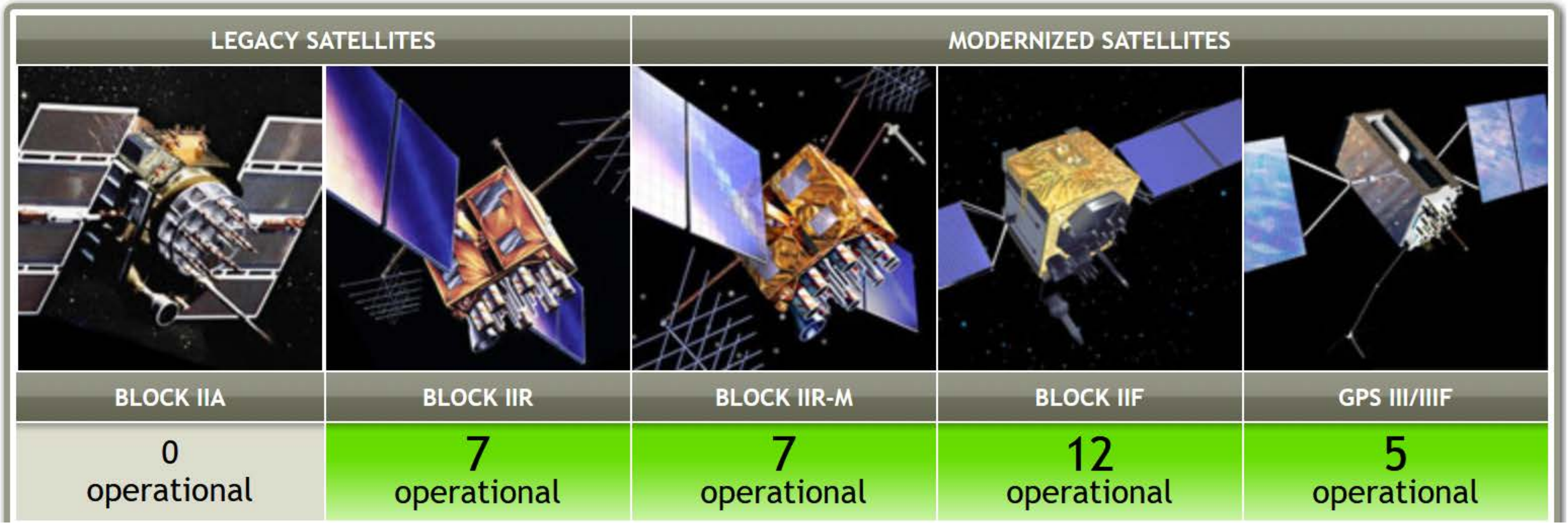

LEGACY SATELLITES		MODERNIZED SATELLITES		
BLOCK IIA	BLOCK IIR	BLOCK IIR-M	BLOCK IIF	GPS III/IIIF
0 operational	7 operational	7 operational	12 operational	5 operational

https://www.gps.gov/systems/gps/space/

Global Network of the IGS

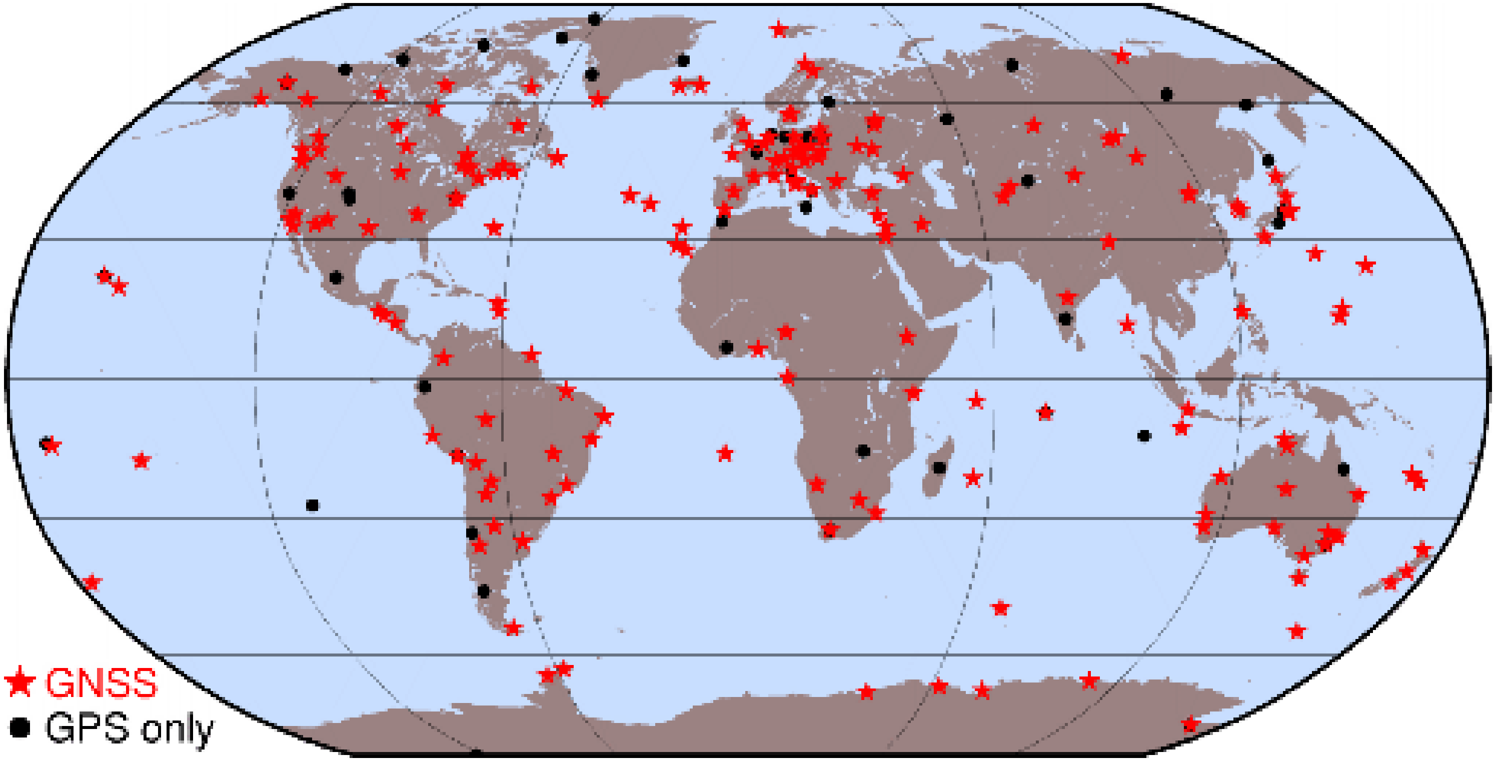

IGS stations used for computation of final orbits at CODE (Dach et al., 2009)

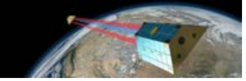

Performance of IGS Final Orbits

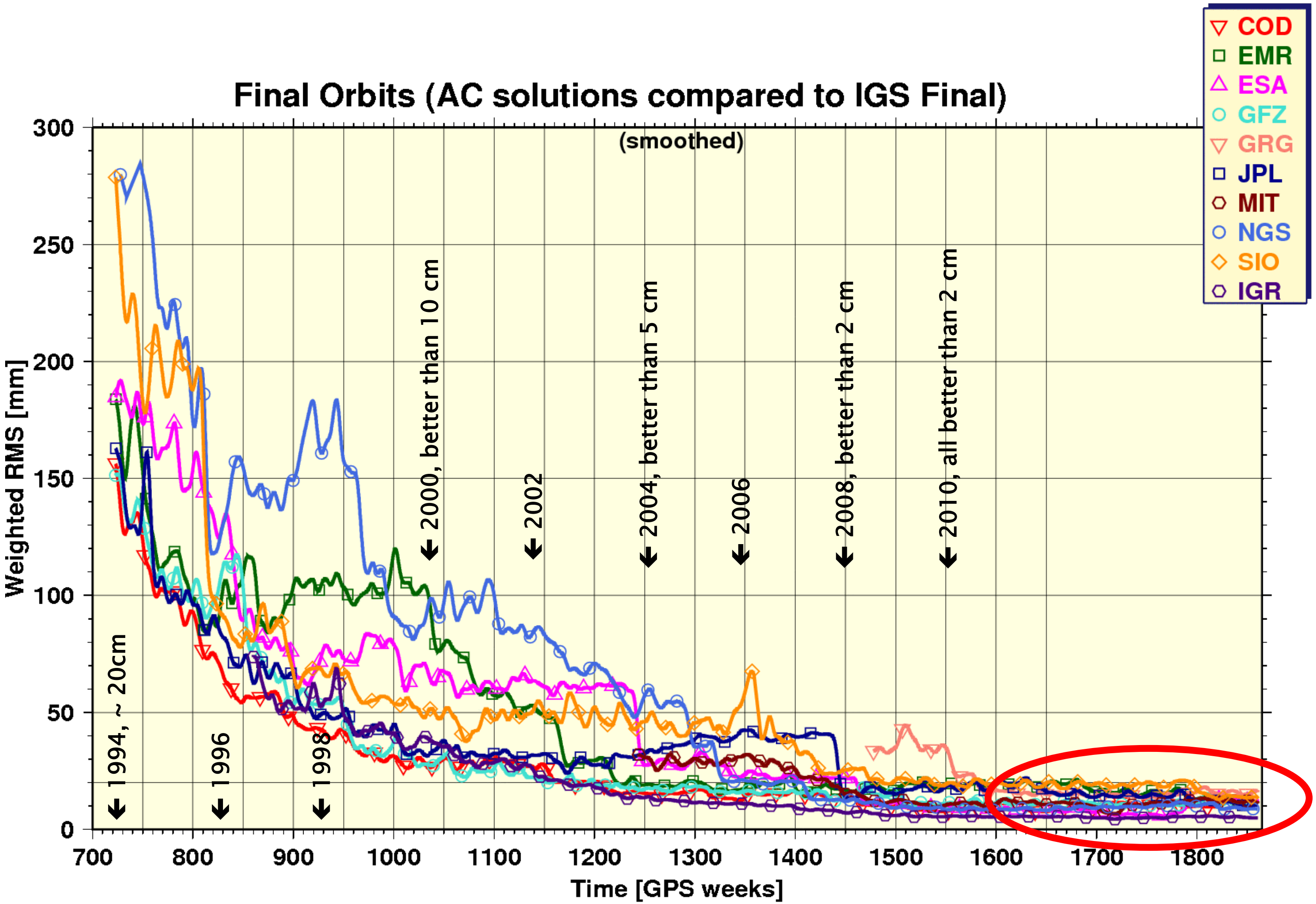

NOAA NGS, 19.09.2015 19:19 (GMT)

http://acc.igs.org/

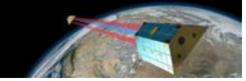

Computation of High-Rate Clocks

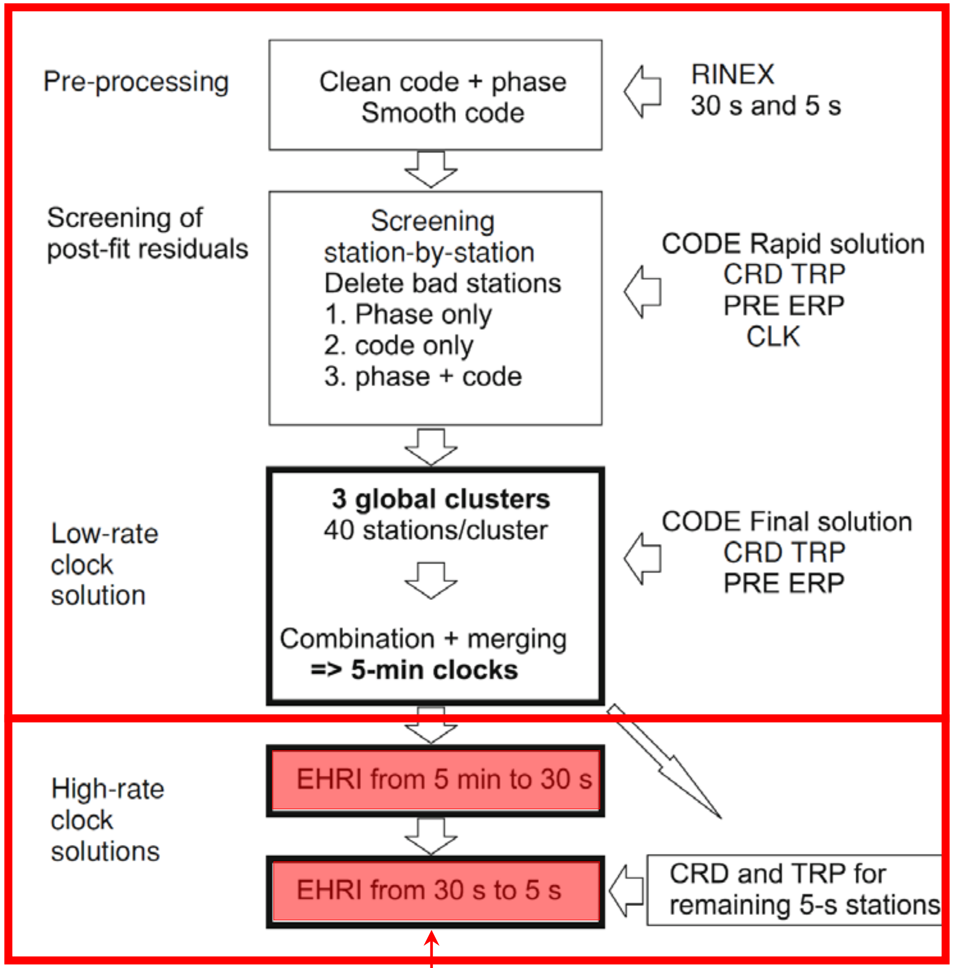

Pre-processing
Clean code + phase
Smooth code
RINEX
30 s and 5 s

Screening of post-fit residuals
Screening
station-by-station
Delete bad stations
1. Phase only
2. code only
3. phase + code
CODE Rapid solution
CRD TRP
PRE ERP
CLK

Low-rate clock solution
3 global clusters
40 stations/cluster
Combination + merging
=> 5-min clocks
CODE Final solution
CRD TRP
PRE ERP

High-rate clock solutions
EHRI from 5 min to 30 s
EHRI from 30 s to 5 s
CRD and TRP for remaining 5-s stations

(Bock et al., 2009)

The final clock product with 5 min sampling is based on undifferenced GPS data of typically 120 stations of the IGS network

The IGS 1 Hz network is finally used for clock densification to 5 sec

The 5 sec clocks are interpolated to 1 sec as needed for 1 Hz kinematic LEO POD

GPS Signals

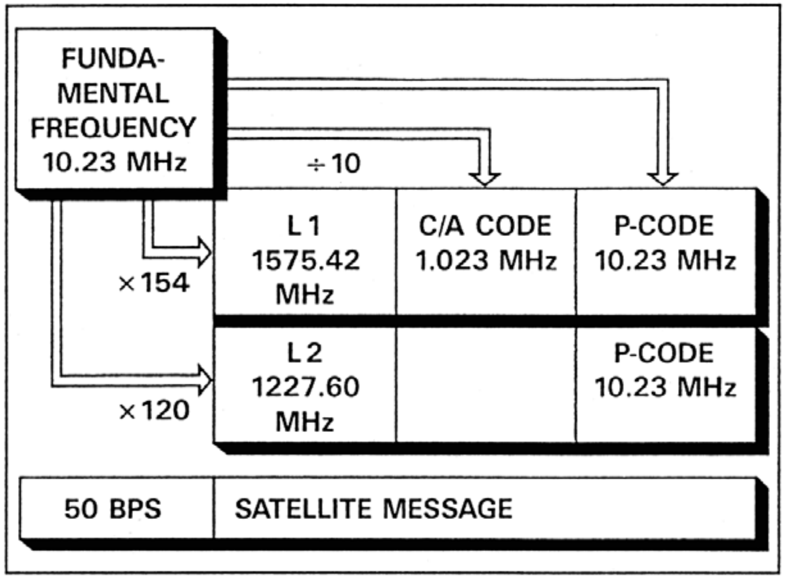
FUNDA-
MENTAL
FREQUENCY
10.23 MHz
÷10
×154
×120
L1
1575.42
MHz
C/A CODE
1.023 MHz
P-CODE
10.23 MHz
L2
1227.60
MHz
P-CODE
10.23 MHz
50 BPS
SATELLITE MESSAGE

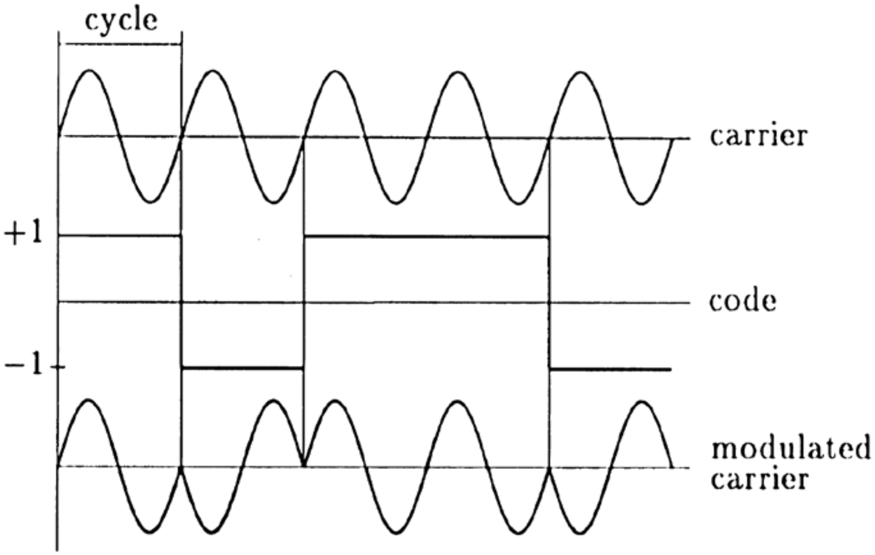
cycle
carrier
+1
−1
code
modulated
carrier

Signals driven by an **atomic clock**

Two **carrier signals** (sine waves):

- **L1**: f = 1575.43 MHz, λ = 19 cm
- **L2**: f = 1227.60 MHz, λ = 24 cm

Bits encoded on carrier by phase modulation:

- **C/A-code** (Clear Access / Coarse Acquisition)
- **P-code** (Protected / Precise)
- **Broadcast/Navigation Message**

Pseudorange / Code Measurements

Code Observations P_i^k are defined as:

$$P_i^k \doteq c\,(T_i - T^k)$$

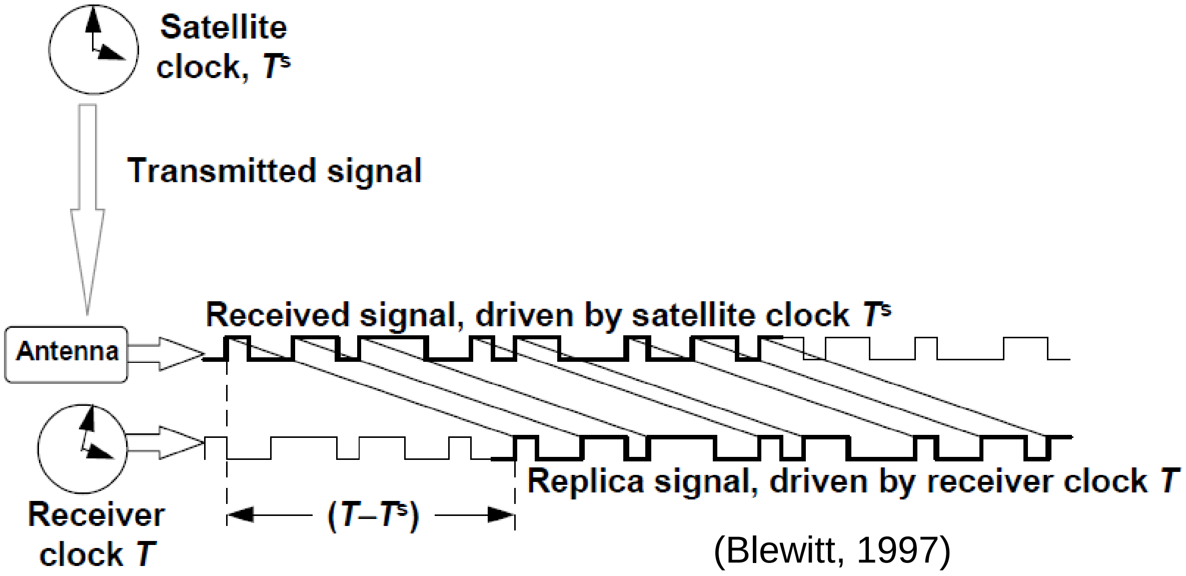
Satellite clock, T^s
Transmitted signal
Received signal, driven by satellite clock T^s
Antenna
Replica signal, driven by receiver clock T
$(T - T^s)$
Receiver clock T

(Blewitt, 1997)
(Teunissen & Montenbruck, 2017)

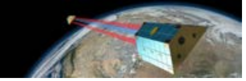

Code Observation Equation

$$P_i^k = \rho_i^k - c \cdot \Delta t^k + c \cdot \Delta t_i$$

t_i, t^k	GPS time of reception and emission
Δt^k	Satellite clock offset $T^k - t^k$
Δt_i	Receiver clock offset $T_i - t_i$
ρ_i^k	Distance between receiver and satellite $c\,(t_i - t^k)$

Known from ACs or IGS:

- satellite positions $(x^{k_j}, y^{k_j}, z^{k_j})$
- satellite clock offsets Δt^{k_j}

4 unknown parameters:

- receiver position (x_i, y_i, z_i)
- receiver clock offset Δt_i

Carrier Phase Measurements (1)

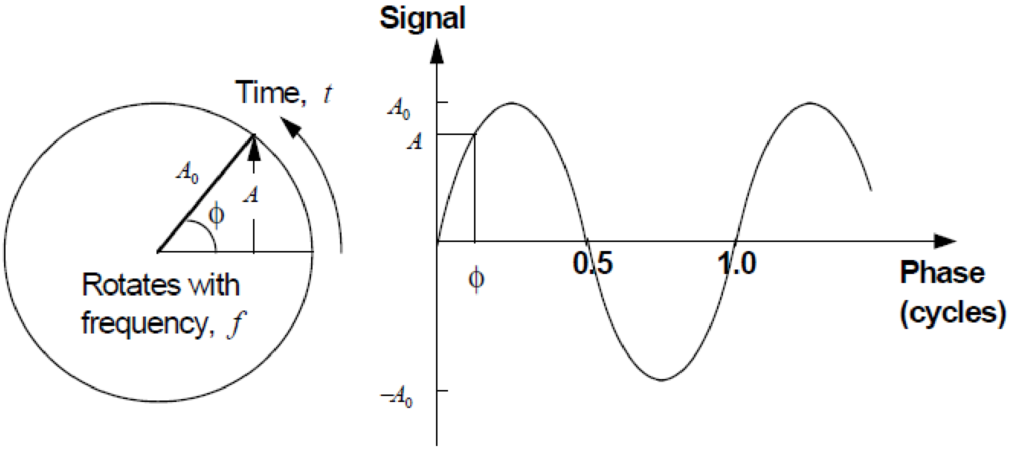
Time, t
A_0
A
ϕ
Rotates with frequency, f
Signal
A_0
A
$-A_0$
ϕ
0.5
1.0
Phase (cycles)

Phase ϕ (in cycles) increases linearly with time t :

$$\phi = f \cdot t$$

where f is the frequency

The **satellite** generates with its clock the phase signal ϕ^k. At emission time T^k (in satellite clock time) we have

$$\phi^k = f \cdot T^k$$

The same phase signal, e.g., a wave crest, propagates from the satellite to the receiver, but the receiver measures only the fractional part of the phase and does not know the **integer number of cycles** N_i^k (phase ambiguity):

$$\phi_i^k = \phi^k - N_i^k = f \cdot T^k - N_i^k$$

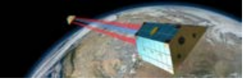

Carrier Phase Measurements (2)

The **receiver** generates with its clock a **reference phase.** At time of reception T_i of the satellite phase ϕ_i^k (in receiver clock time) we have:

$$\phi_i = f \cdot T_i$$

The actual **phase measurement** is the difference between receiver reference phase ϕ_i and satellite phase ϕ_i^k:

$$\psi_i^k = \phi_i - \phi_i^k = f \cdot T_i - (f \cdot T^k - N_i^k) = f \cdot (T_i - T^k) + N_i^k$$

Multiplication with the wavelength $\lambda = c/f$ leads to the **phase observation equation** in meters:

$$\begin{aligned} L_i^k &= \lambda \cdot \psi_i^k = c \cdot (T_i - T^k) + \lambda \cdot N_i^k \\ &= \rho_i^k - c \cdot \Delta t^k + c \cdot \Delta t_i + \lambda \cdot N_i^k \end{aligned}$$

Difference to the pseudorange observation: **integer ambiguity term** N_i^k

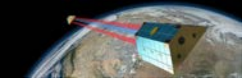

Detailed Observation Equation

$$L_i^k = \rho_i^k - c \cdot \Delta t^k + c \cdot \Delta t_i + \xcancel{T_i^k} + \xcancel{I_i^k} + \lambda \cdot N_i^k$$
$$+ \Delta_{rel} - c \cdot b^k + c \cdot b_i + m_i^k + \epsilon_i^k$$

ρ_i^k	Distance between satellite and receiver
Δt^k	Satellite clock offset wrt GPS time
Δt_i	Receiver clock offset wrt GPS time
~~T_i^k~~	~~Tropospheric delay~~
~~I_i^k~~	~~Ionospheric delay~~
N_i^k	Phase ambiguity
Δ_{rel}	Relativistic corrections
b^k	Delays in satellite (cables, electronics)
b_i	Delays in receiver and antenna
m_i^k	Multipath, scattering, bending effects
ϵ_i^k	Measurement error

Satellite positions and clocks are known from the IGS

Not existent for LEOs

Cancels out (first order only) when forming the ionosphere-free linear combination:

$$L_c = \frac{f_1^2}{f_1^2 - f_2^2} L_1 - \frac{f_2^2}{f_1^2 - f_2^2} L_2$$

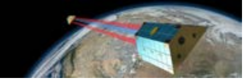

Geometric Distance

Geometric distance ρ_{leo}^{k} is given by:

$$\rho_{leo}^{k} = \left|\boldsymbol{r}_{leo}(t_{leo}) - \boldsymbol{r}^{k}(t_{leo} - \tau_{leo}^{k})\right|$$

$\boldsymbol{r}_{leo}$	Inertial position of LEO antenna phase center at reception time
$\boldsymbol{r}^{k}$	Inertial position of GPS antenna phase center of satellite k at emission time
τ_{leo}^{k}	Signal traveling time between the two phase center positions

Different ways to represent $\boldsymbol{r}_{leo}$:

- **Kinematic** orbit representation
- **Dynamic** or **reduced-dynamic** orbit representation

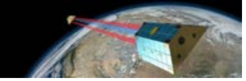

Different Orbit Representations

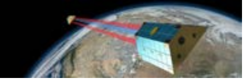

Kinematic Orbit Representation (1)

Satellite position $\boldsymbol{r}_{leo}(t_{leo})$ (in inertial frame) is given by:

$$\boldsymbol{r}_{leo}(t_{leo}) = \boldsymbol{R}(t_{leo}) \cdot (\boldsymbol{r}_{leo,e,0}(t_{leo}) + \delta\boldsymbol{r}_{leo,e,ant}(t_{leo}))$$

$\boldsymbol{R}$	Transformation matrix from Earth-fixed to inertial frame
$\boldsymbol{r}_{leo,e,0}$	LEO center of mass position in Earth-fixed frame
$\delta\boldsymbol{r}_{leo,e,ant}$	LEO antenna phase center offset in Earth-fixed frame

Kinematic positions $\boldsymbol{r}_{leo,e,0}$ are estimated for each **measurement epoch**:

- Measurement epochs **need not** to be identical with nominal epochs
- Positions are **independent** of models describing the LEO dynamics. Velocities and accelerations cannot be provided in a "strict" sense.

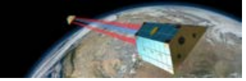

Kinematic Orbit Representation (2)

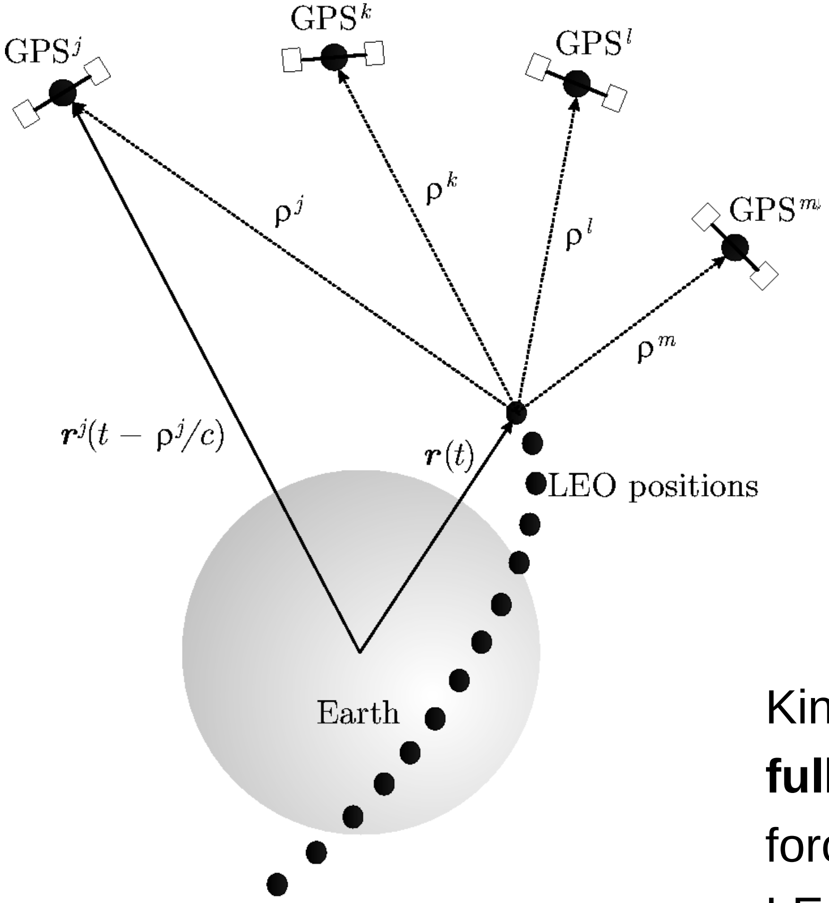
GPS^j
GPS^k
GPS^l
GPS^m
ρ^j
ρ^k
ρ^l
ρ^m
$\boldsymbol{r}^j(t-\rho^j/c)$
$\boldsymbol{r}(t)$
LEO positions
Earth

A kinematic orbit is an ephemeris at **discrete** measurement epochs

Kinematic positions are **fully independent** on the force models used for LEO orbit determination

(Svehla and Rothacher, 2004)

Kinematic Orbit Representation (3)

Measurement epochs
(in GPS time)

Positions (km)
(Earth-fixed)

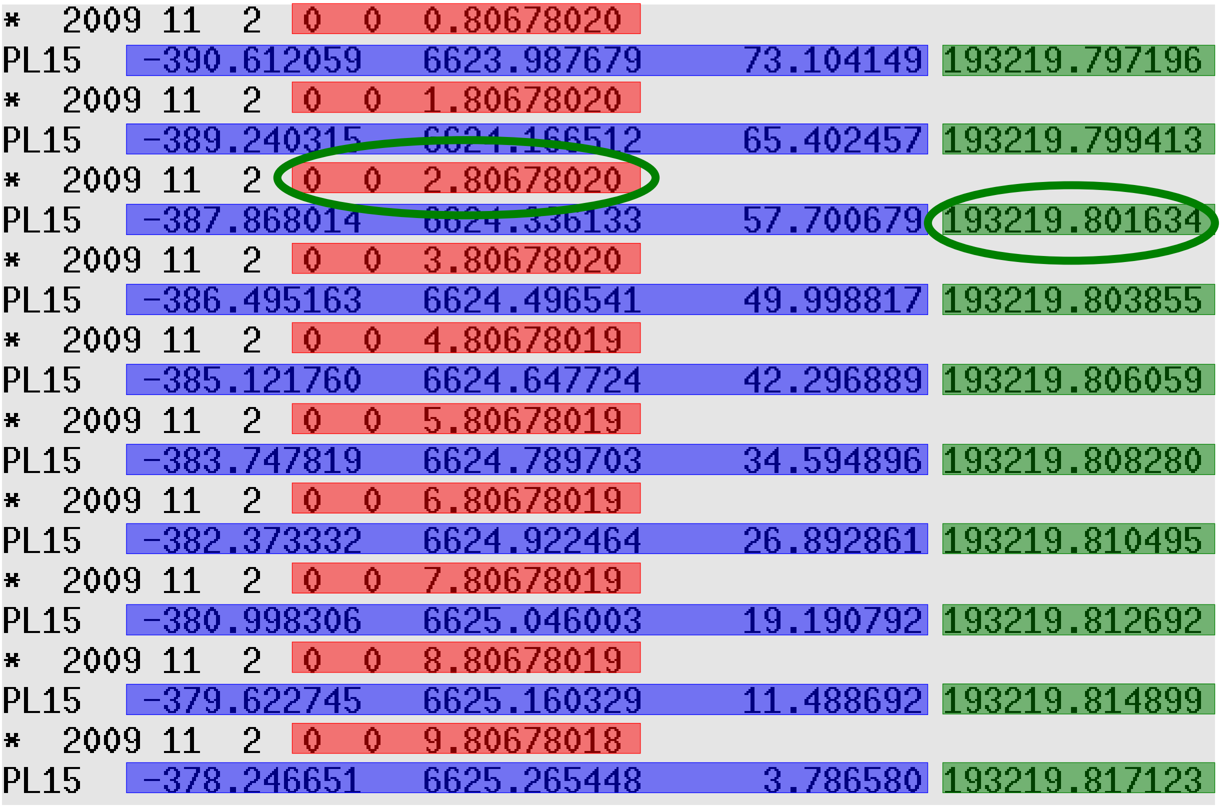

```
*  2009 11  2  0  0  0.80678020
PL15  -390.612059   6623.987679     73.104149 193219.797196
*  2009 11  2  0  0  1.80678020
PL15  -389.240315   6624.166512     65.402457 193219.799413
*  2009 11  2  0  0  2.80678020
PL15  -387.868014   6624.336133     57.700679 193219.801634
*  2009 11  2  0  0  3.80678020
PL15  -386.495163   6624.496541     49.998817 193219.803855
*  2009 11  2  0  0  4.80678019
PL15  -385.121760   6624.647724     42.296889 193219.806059
*  2009 11  2  0  0  5.80678019
PL15  -383.747819   6624.789703     34.594896 193219.808280
*  2009 11  2  0  0  6.80678019
PL15  -382.373332   6624.922464     26.892861 193219.810495
*  2009 11  2  0  0  7.80678019
PL15  -380.998306   6625.046003     19.190792 193219.812692
*  2009 11  2  0  0  8.80678019
PL15  -379.622745   6625.160329     11.488692 193219.814899
*  2009 11  2  0  0  9.80678018
PL15  -378.246651   6625.265448      3.786580 193219.817123
```

Clock correction to nominal epoch (µs), e.g., to epoch 00:00:03

Excerpt of kinematic GOCE positions at begin of 2 Nov, 2009

Recovery of Large-Scale Time-Variable Gravity Signals

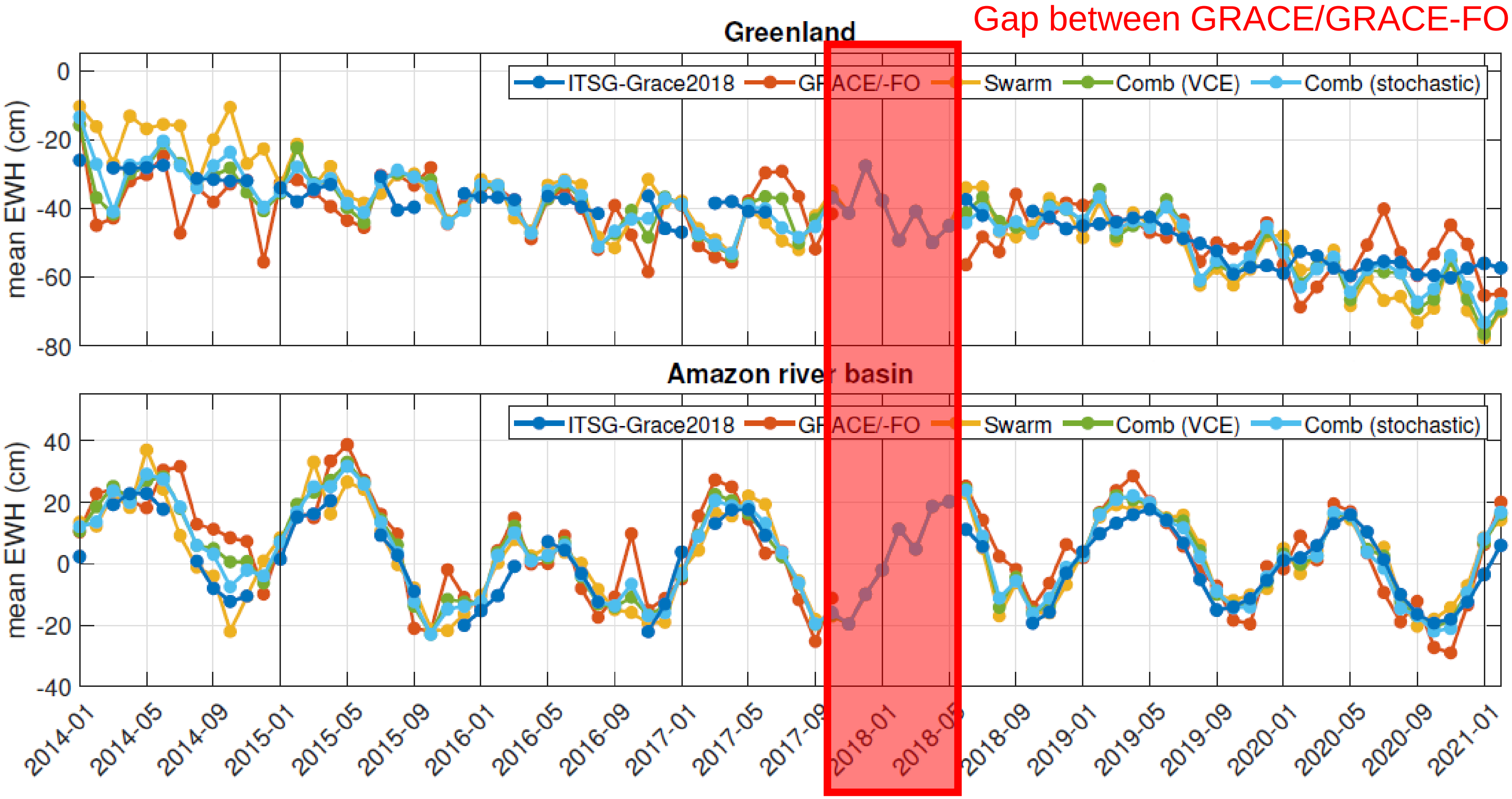

Kinematic positions allow it to recover the **long wavelength** part of the Earth's time-variable gravity field. The scatter of monthly gravity field solutions is larger than from dedicated GRACE/GRACE-FO data, but trends and annual signals may be derived remarkably well.

(Grombein et al., 2022)

Example: Sentinel-3A GPS Tracking

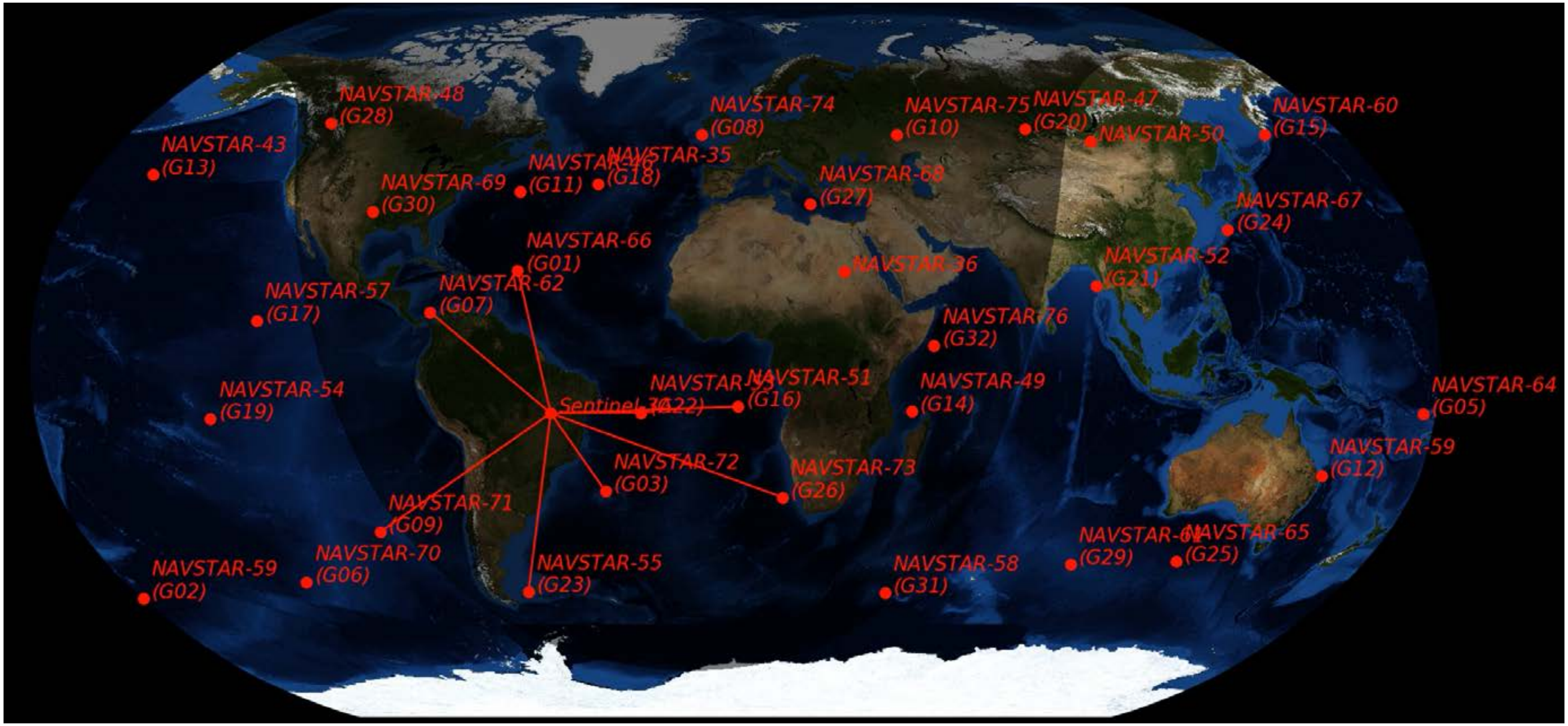
NAVSTAR-48 (G28)
NAVSTAR-43 (G13)
NAVSTAR-74 (G08)
NAVSTAR-75 (G10)
NAVSTAR-47 (G20)
NAVSTAR-50
NAVSTAR-60 (G15)
NAVSTAR-69 (G30)
NAVSTAR-46 (G11)
NAVSTAR-35 (G18)
NAVSTAR-68 (G27)
NAVSTAR-67 (G24)
NAVSTAR-66 (G01)
NAVSTAR-36
NAVSTAR-52 (G21)
NAVSTAR-57 (G17)
NAVSTAR-62 (G07)
NAVSTAR-76 (G32)
NAVSTAR-54 (G19)
Sentinel-3A
NAVSTAR-53 (G22)
NAVSTAR-51 (G16)
NAVSTAR-49 (G14)
NAVSTAR-64 (G05)
NAVSTAR-72 (G03)
NAVSTAR-73 (G26)
NAVSTAR-59 (G12)
NAVSTAR-71 (G09)
NAVSTAR-61 (G29)
NAVSTAR-65 (G25)
NAVSTAR-70 (G06)
NAVSTAR-59 (G02)
NAVSTAR-55 (G23)
NAVSTAR-58 (G31)

Example: Sentinel-6A multi-GNSS Tracking

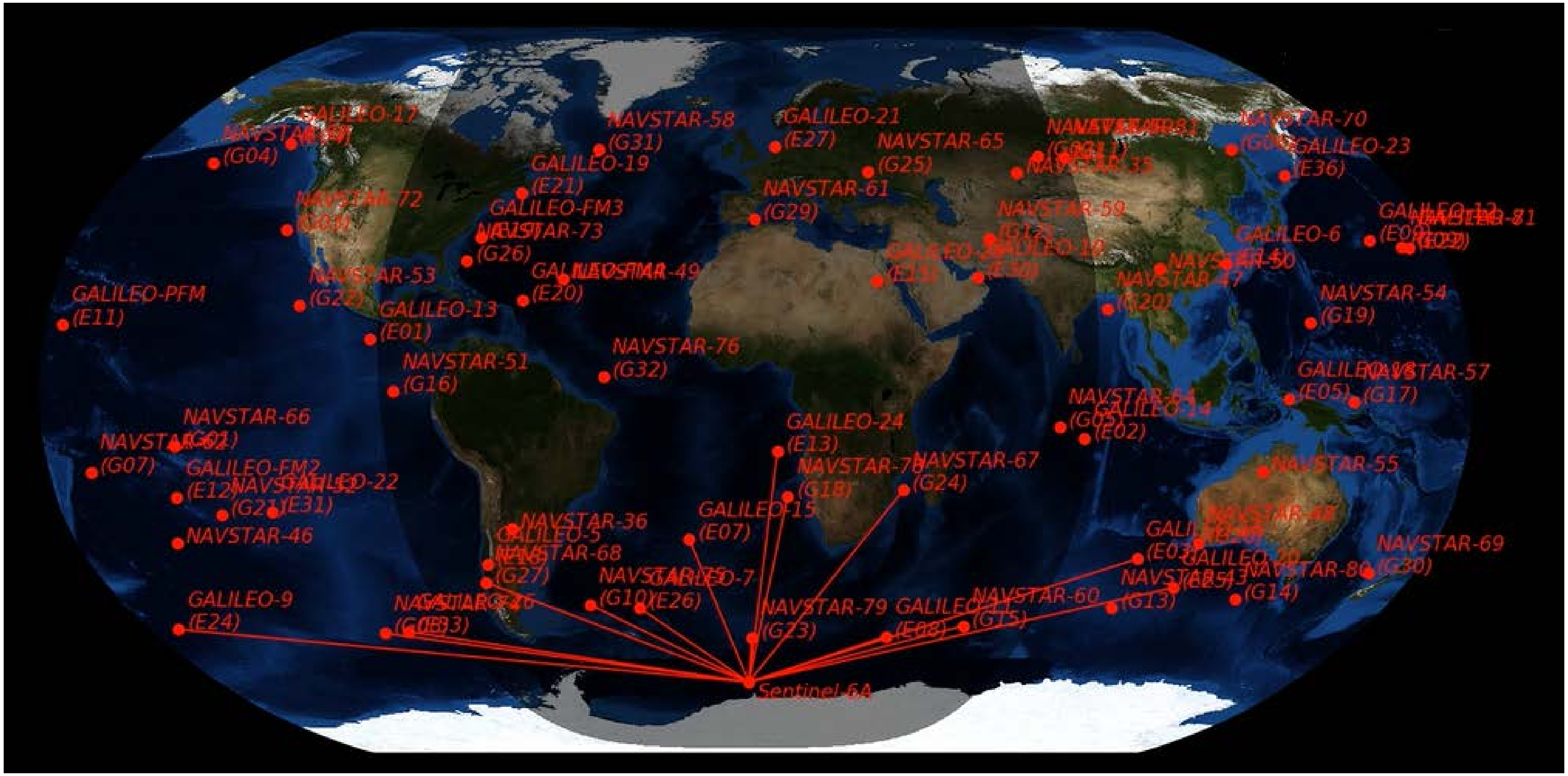
GALILEO-17
(G04)
NAVSTAR-58
(G31)
GALILEO-21
(E27)
NAVSTAR-65
(G25)
NAVSTAR-70
GALILEO-23
(E36)
NAVSTAR-35
GALILEO-19
(E21)
NAVSTAR-61
(G29)
NAVSTAR-72
GALILEO-FM3
NAVSTAR-73
(G26)
NAVSTAR-59
GALILEO-6
NAVSTAR-49
(E20)
(E15)
(E30)
NAVSTAR-50
NAVSTAR-47
(G20)
NAVSTAR-53
(G22)
GALILEO-PFM
(E11)
GALILEO-13
(E01)
NAVSTAR-54
(G19)
NAVSTAR-76
(G32)
NAVSTAR-51
(G16)
NAVSTAR-57
(E05)
(G17)
GALILEO-14
(E02)
NAVSTAR-66
(G07)
GALILEO-FM2
GALILEO-22
(E31)
GALILEO-24
(E13)
NAVSTAR-67
(G24)
(G18)
NAVSTAR-55
NAVSTAR-46
NAVSTAR-36
GALILEO-5
NAVSTAR-68
(G27)
GALILEO-15
(E07)
NAVSTAR-48
NAVSTAR-69
(G30)
GALILEO-7
(G10)
(E26)
NAVSTAR-80
(G14)
GALILEO-9
(E24)
NAVSTAR-79
(G23)
NAVSTAR-60
(G13)
(G15)
(E08)
Sentinel-6A

Simulated Data Set (1)

The simplified **Code Observation Equation** of the simulation reads as

$$\bar{\rho}_{k,i} = \sqrt{(x_{k,i} - x_{leo,i})^2 + (y_{k,i} - y_{leo,i})^2 + (z_{k,i} - z_{leo,i})^2} + c_{leo,i} \quad , \quad k = 1, \ldots, n_{sat}$$

with

$(x_{k,i}, y_{k,i}, z_{k,i})$	Known inertial position of GPS satellite *k* at epoch *i*
$(x_{leo,i}, y_{leo,i}, z_{leo,i})$	Unknown inertial LEO position at epoch *i*
$c_{leo,i}$	Unknown clock correction of LEO receiver at epoch *i*

The simplified **Phase Observation Equation** of the simulation reads as

$$\bar{\lambda}_{k,i} = \sqrt{(x_{k,i} - x_{leo,i})^2 + (y_{k,i} - y_{leo,i})^2 + (z_{k,i} - z_{leo,i})^2} + c_{leo,i} + b_k \quad , \quad k = 1, \ldots, n_{sat}$$

with the additional parameter

b_k	Unknown constant phase bias to the satellite *k*

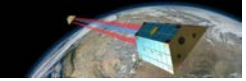

Simulated Data Set (2)

Tabelle 1: Code observations $\rho'_{k,i}$ contained in the file `OBS_CODE.txt`. They are stored in `template.m` in the array `obs_code(kepo,isat)`. In analogy the phase observations are contained in the file `OBS_PHASE.txt` and are stored in the array `obs_phase(kepo,isat)`. The observation times are also computed in the source code by `t = 10*(kepo-1)`, kepo $= 1, \ldots,$ nepo.

Time t_i (sec)	Sat. 1 (m)	Sat. 2 (m)	Sat. 3 (m)	Sat. 4 (m)	Sat. 5 (m)	etc.
0.0000	19447557.3266	0.0000	0.0000	0.0000	21654965.4010	...
10.0000	19446601.2222	0.0000	0.0000	0.0000	21678374.5718	...
20.0000	19446475.1291	0.0000	0.0000	0.0000	21702249.7103	...
...	...	...	...	...	....	...

Tabelle 2: Positions $(x_{k,i}, y_{k,i}, z_{k,i})$ of the GPS satellites contained in the file `GPS.txt`. They are stored in the array `r_gps(coord,iepo,ksat)`.

x GPS 1 (m)	y GPS 1 (m)	z GPS 1 (m)	x GPS 2	y GPS 2	z GPS 2	etc.
26235000.0000	0.0000	0.0000	-789889.9012	-15196033.7951	-21702185.3748	...
26234971.0435	22468.8157	32088.7944	-751120.9506	-15196458.0361	-21702791.2539	...
26234884.1742	44937.5818	64177.5179	-712350.3922	-15196849.7458	-21703350.6732	...
...	...	...	...	...	....	...

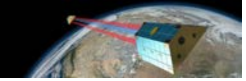

Simulated Data Set (3)

Tabelle 3: Positions $(x_{leo,i}, y_{leo,i}, z_{leo,i})$ and velocities of the LEO satellite contained in the file `LEO.txt`. The positions are stored in the array `r_leo(coord,iepo)`. The velocities are not needed for this project unless the orbit differences shall be plotted in a radial, along-track, cross-track frame instead of the inertial x,y,z frame.

x LEO (m)	y LEO (m)	z LEO (m)	v_x LEO (m/s)	v_y LEO (m/s)	v_z LEO (m/s)
6824717.7284	1203381.8712	0.0000	-0.0000	0.0000	7621.8949
6824309.0437	1203309.8091	76217.4278	-81.7361	-14.4123	7621.4385
6823083.0403	1203093.6316	152425.7274	-163.4621	-28.8228	7620.0693
...	...	...	...	...	...

Tabelle 4: Biases b_k of the phase observations to satellite k contained in the file `BIASES.txt`. They are stored in the array `true_bias(ksat)`.

b_1 (m)	b_2 (m)	b_3 (m)	b_4 (m)	etc.
2319	-1149	2918	-10144	...

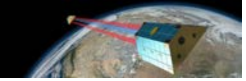

Simulated Data Set (4)

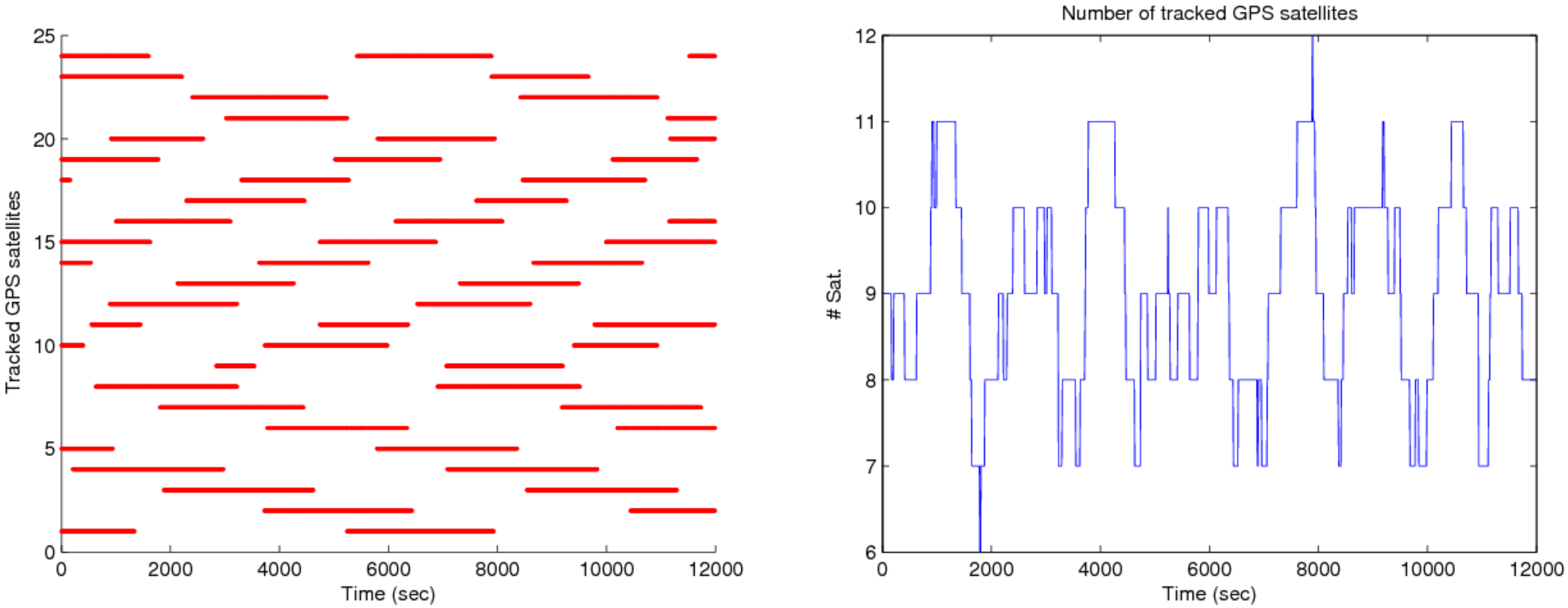

Tracking scenario of the simulated data set (left). Up to 12 GPS satellites are at maximum simultaneously visible from the LEO satellite (right). The viewing geometry is continuously changing due to the orbital motion of all satellites.

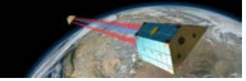

Dynamic Orbit Representation (1)

Satellite position $\boldsymbol{r}_{leo}(t_{leo})$ (in inertial frame) is given by:

$$\boldsymbol{r}_{leo}(t_{leo}) = \boldsymbol{r}_{leo,0}(t_{leo}; a, e, i, \Omega, \omega, u_0; Q_1, ..., Q_d) + \delta\boldsymbol{r}_{leo,ant}(t_{leo})$$

$\boldsymbol{r}_{leo,0}$	LEO center of mass position
$\delta\boldsymbol{r}_{leo,ant}$	LEO antenna phase center offset
$a, e, i, \Omega, \omega, u_0$	LEO initial osculating orbital elements
$Q_1, ..., Q_d$	LEO dynamical parameters

Satellite trajectory $\boldsymbol{r}_{leo,0}$ is a particular solution of an **equation of motion**

- One set of **initial conditions** (orbital elements) is estimated per arc. Dynamical parameters of the force model may be estimated on request.

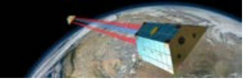

Dynamic Orbit Representation (2)

Equation of motion (in inertial frame) is given by:

$$\ddot{\boldsymbol{r}} = -GM\frac{\boldsymbol{r}}{r^3} + \boldsymbol{f}_1(t, \boldsymbol{r}, \dot{\boldsymbol{r}}, Q_1, ..., Q_d)$$

with initial conditions

$$\begin{aligned} \boldsymbol{r}(t_0) &= \boldsymbol{r}(a, e, i, \Omega, \omega, u_0; t_0) \\ \dot{\boldsymbol{r}}(t_0) &= \dot{\boldsymbol{r}}(a, e, i, \Omega, \omega, u_0; t_0) \end{aligned}$$

The **acceleration** $\boldsymbol{f}_1$ consists of **gravitational** and **non-gravitational** perturbations taken into account to model the satellite trajectory. Unknown parameters $Q_1, ..., Q_d$ of force models may appear in the equation of motion together with deterministic (known) accelerations given by analytical models.

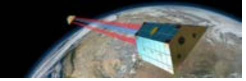

Perturbing Accelerations of a LEO Satellite

Force	Acceleration (m/s²)
Central term of Earth‘s gravity field	8.42
Oblateness of Earth‘s gravity field	0.015
Atmospheric drag	0.00000079
Higher order terms of Earth‘s gravity field	0.00025
Attraction from the Moon	0.0000054
Attraction from the Sun	0.0000005
Direct solar radiation pressure	0.000000097
...	...

Perturbing Accelerations of a LEO Satellite

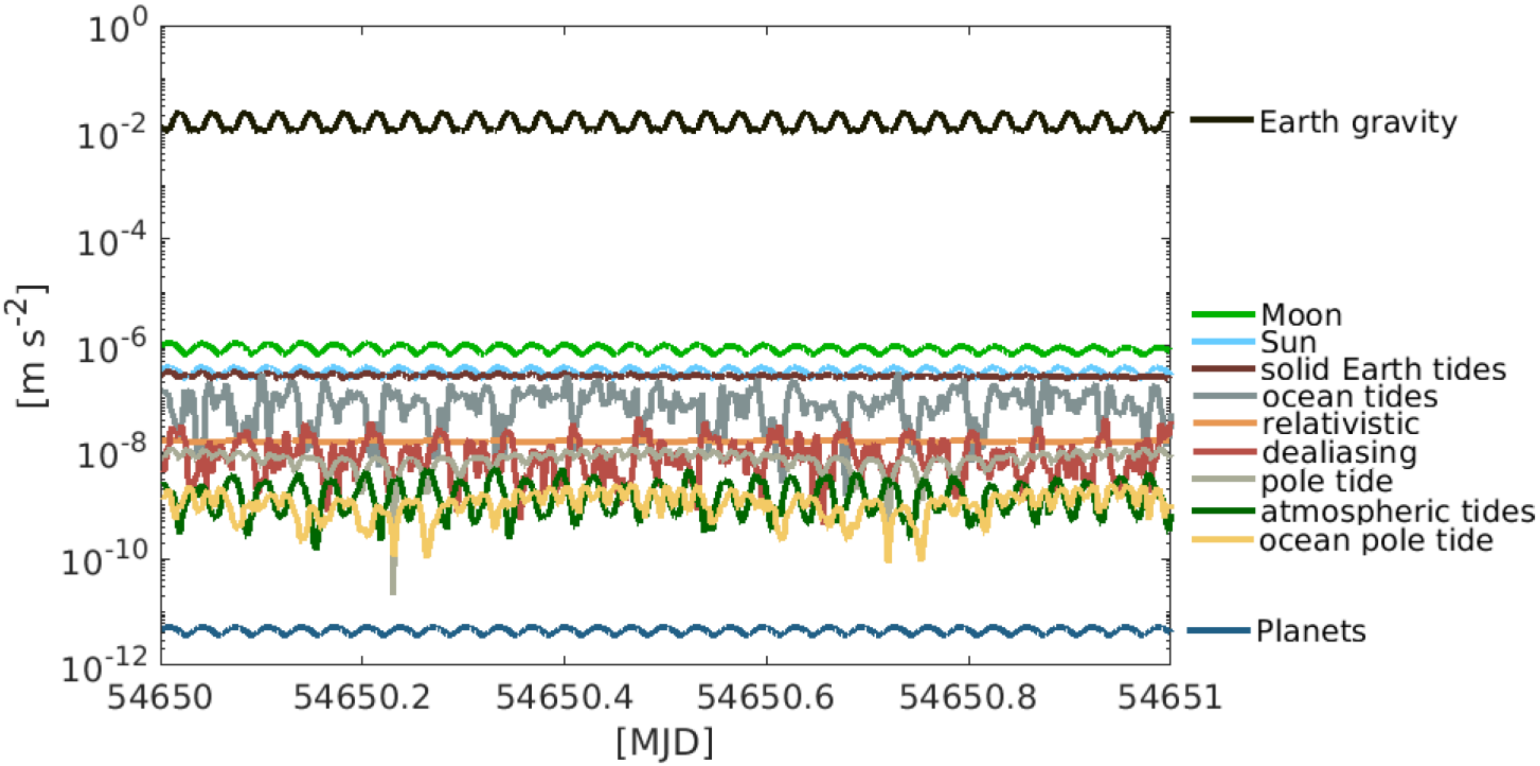

Norm of the **COST-G benchmark accelerations** along a GRACE satellite orbit. The benchmark data set may be used as a reference data set and provides the opportunity to test the implementation of corresponding background models.

(Mayer-Gürr and Kvas, 2019; Lasser et al., 2020)

Osculating Orbital Elements

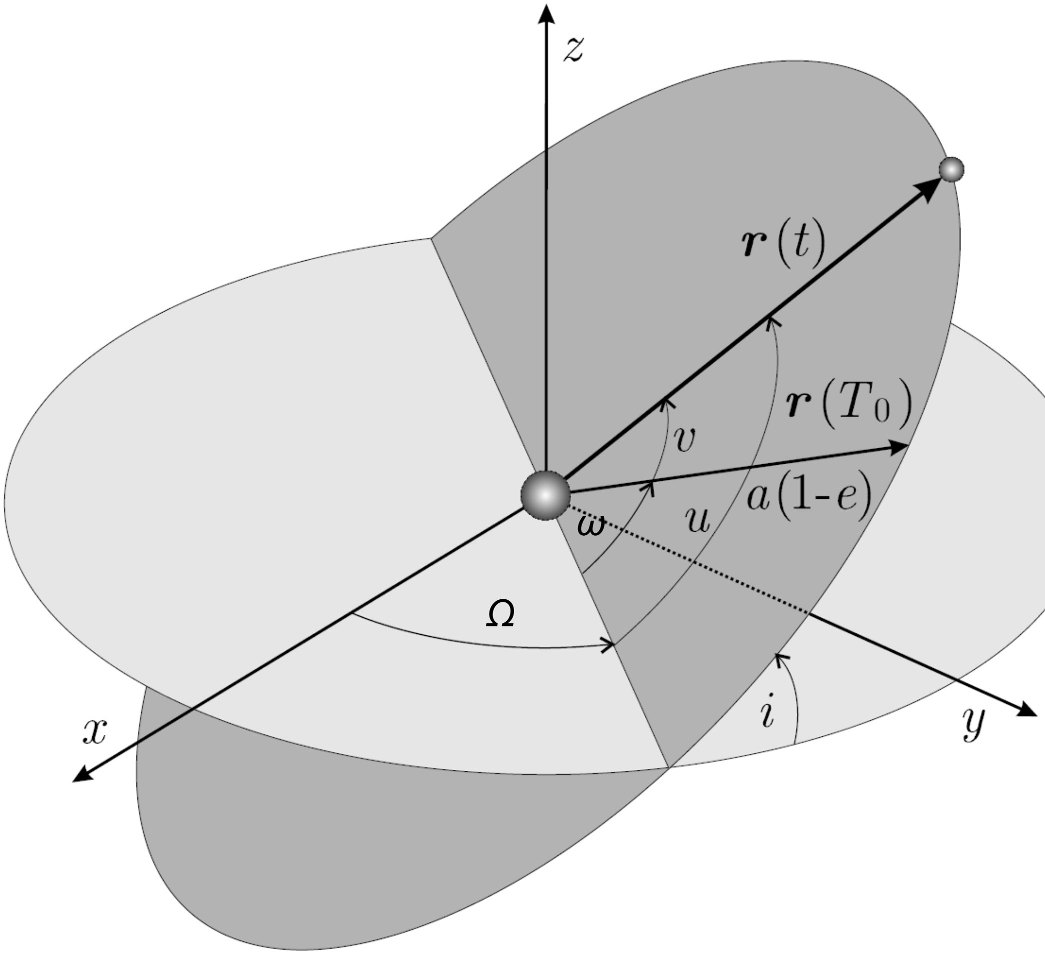
z
$\boldsymbol{r}(t)$
$\boldsymbol{r}(T_0)$
v
$a(1\text{-}e)$
ω
u
Ω
i
x
y

(Beutler, 2005)

Osculating Orbital Elements of GOCE (1)

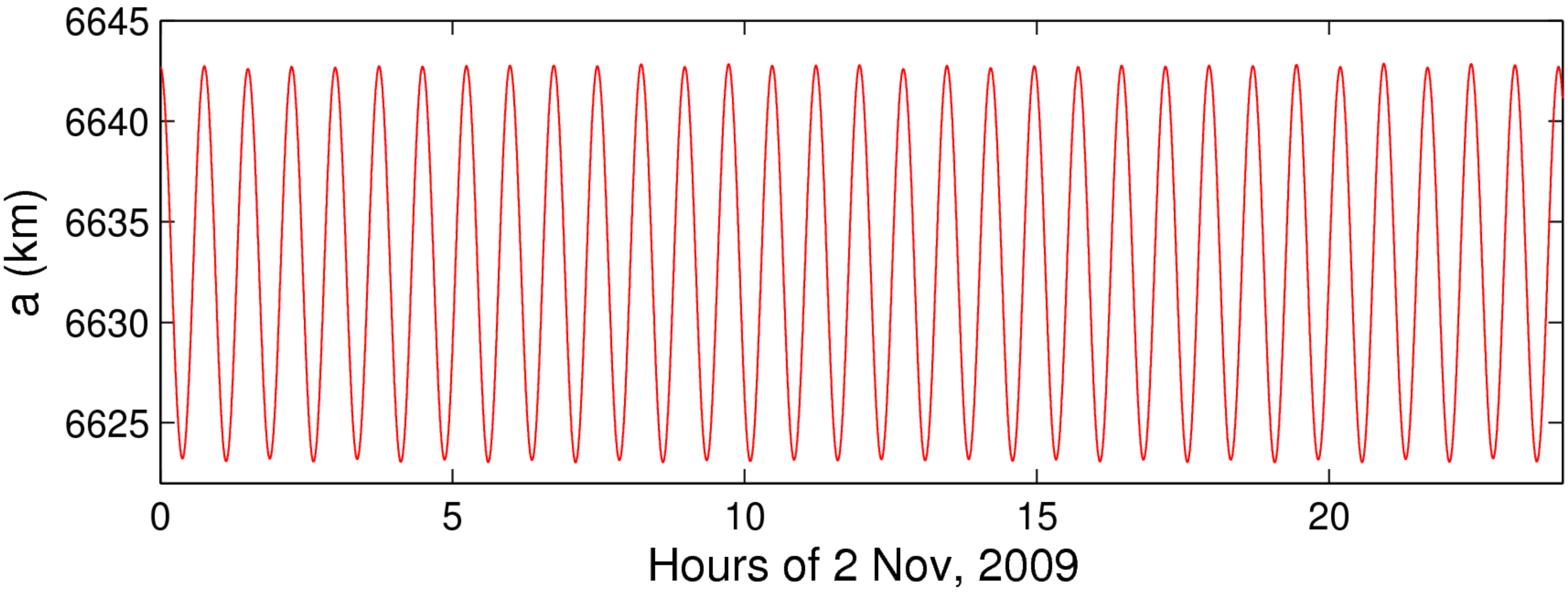

Semi-major axis:

Twice-per-revolution variations of about ±10 km around the mean semi-major axis of 6632.9km, which corresponds to a mean altitude of 254.9 km

Osculating Orbital Elements of GOCE (2)

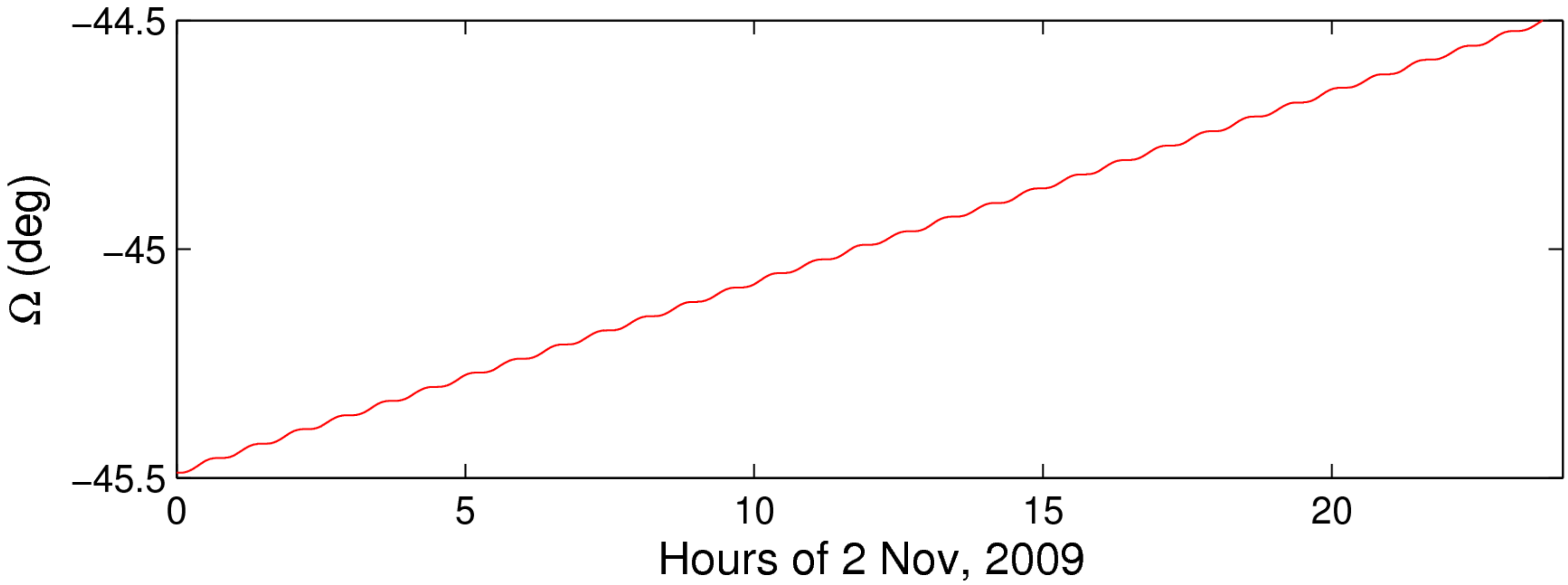

Right ascension of ascending node:

Twice-per-revolution variations and linear drift of about +1°/day (360°/365days) due to the sun-synchronous orbit

Dynamic Orbit Representation (3)

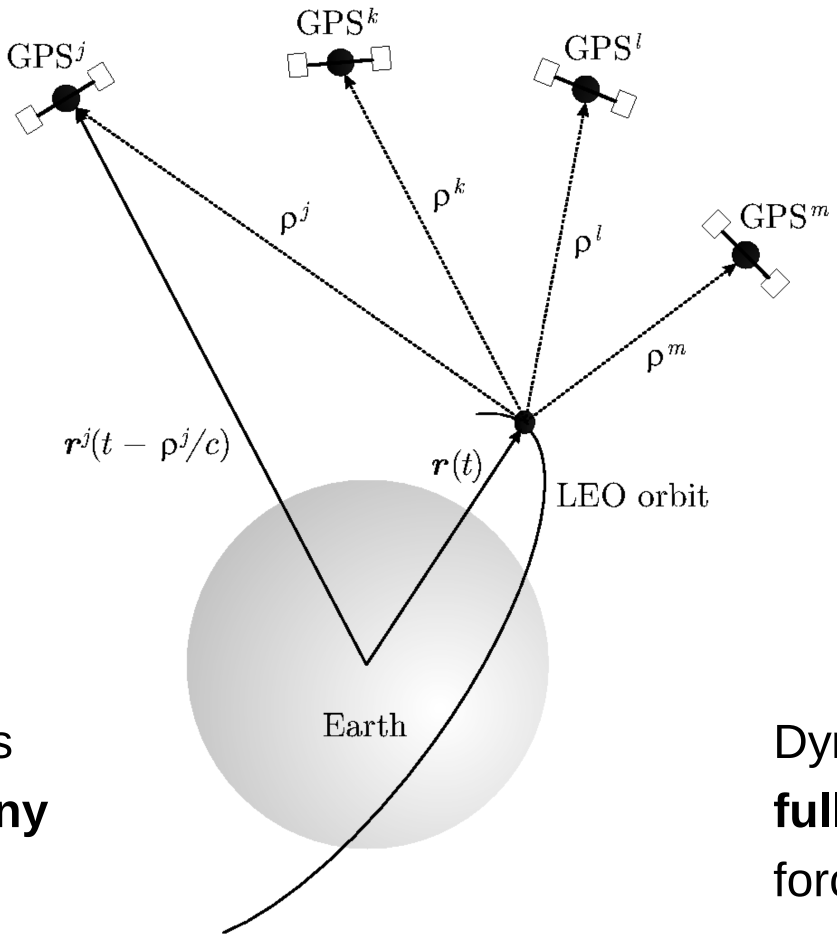
GPS^j
GPS^k
GPS^l
GPS^m
ρ^j
ρ^k
ρ^l
ρ^m
$\boldsymbol{r}^j(t - \rho^j/c)$
$\boldsymbol{r}(t)$
LEO orbit
Earth

Dynamic orbit positions may be computed at **any epoch** within the arc

Dynamic positions are **fully dependent** on the force models used, e.g., on the gravity field model

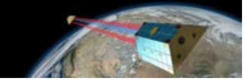

Reduced-Dynamic Orbit Representation (1)

Equation of motion (in inertial frame) is given by:

$$\ddot{\boldsymbol{r}} = -GM\frac{\boldsymbol{r}}{r^3} + \boldsymbol{f}_1(t, \boldsymbol{r}, \dot{\boldsymbol{r}}, Q_1, ..., Q_d, P_1, ..., P_s)$$

$P_1, ..., P_s$ Pseudo-stochastic parameters

Pseudo-stochastic parameters are:

- additional empirical parameters characterized by a priori known **statistical properties**, e.g., by expectation values and a priori variances
- useful to **compensate** for deficiencies in dynamic models, e.g., deficiencies in models describing non-gravitational accelerations
- often set up as **piecewise constant accelerations** to ensure that satellite trajectories are continuous and differentiable at any epoch

Reduced-Dynamic Orbit Representation (2)

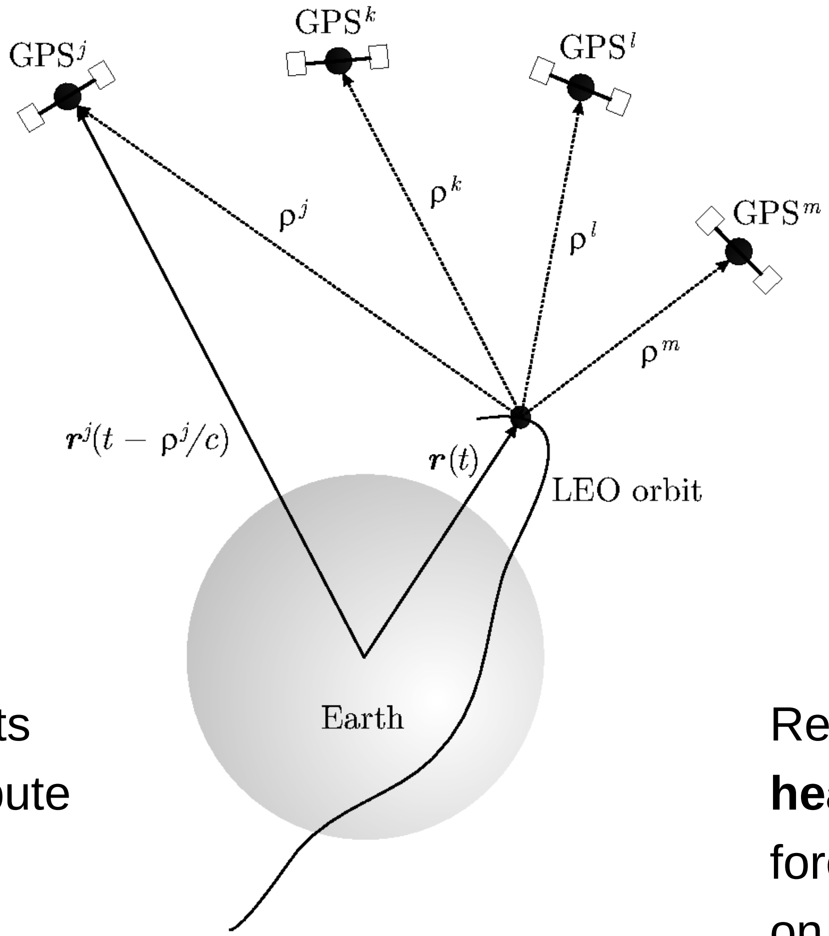
GPS^j
GPS^k
GPS^l
GPS^m
ρ^j
ρ^k
ρ^l
ρ^m
$\boldsymbol{r}^j(t - \rho^j/c)$
$\boldsymbol{r}(t)$
LEO orbit
Earth

Reduced-dynamic orbits are well suited to compute LEO orbits of **highest quality**

(Jäggi et al., 2006; Jäggi, 2007)

Reduced-dynamic orbits **heavily depend** on the force models used, e.g., on the gravity field model

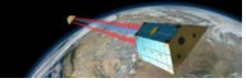

Reduced-dynamic Orbit Representation (3)

Position epochs

(in GPS time)

Positions (km) &

Velocities (dm/s)

(Earth-fixed)

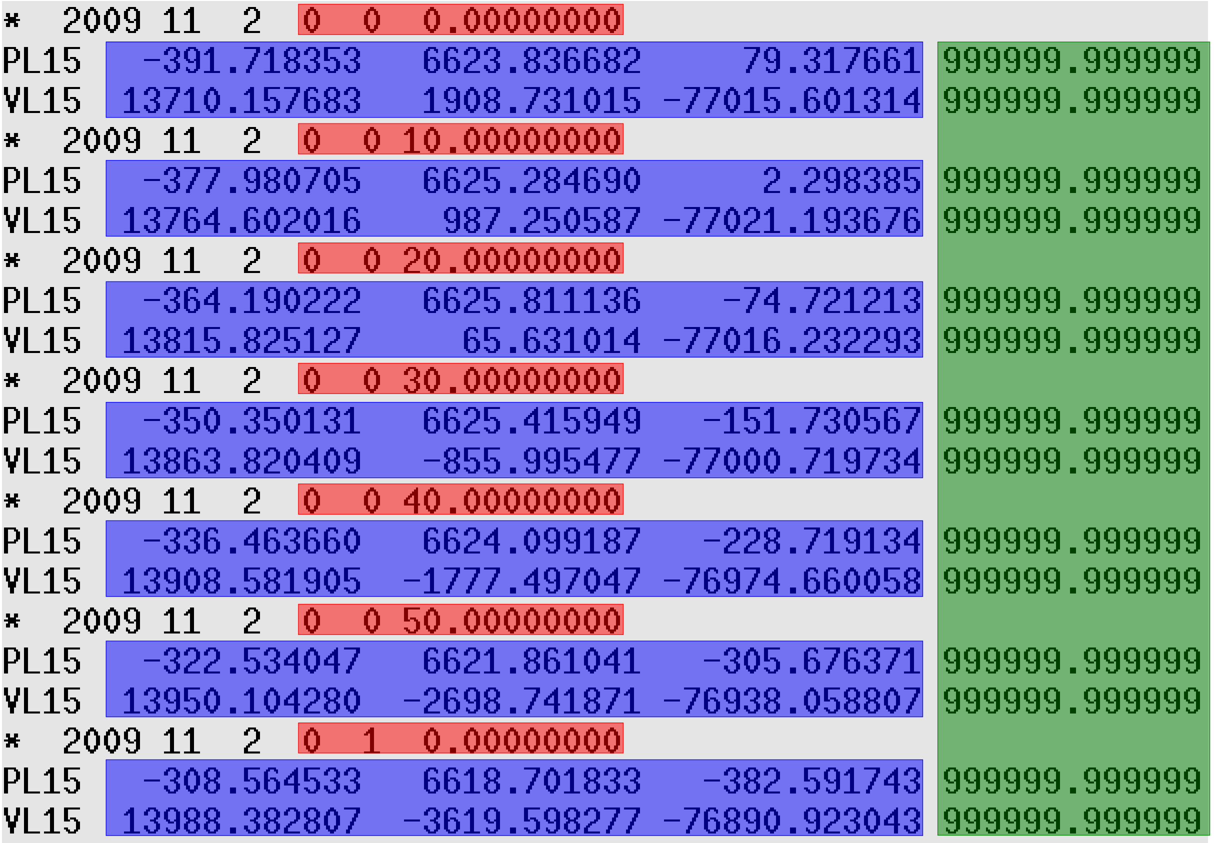

```
*  2009 11  2  0  0  0.00000000
PL15   -391.718353   6623.836682     79.317661 999999.999999
VL15  13710.157683   1908.731015 -77015.601314 999999.999999
*  2009 11  2  0  0 10.00000000
PL15   -377.980705   6625.284690      2.298385 999999.999999
VL15  13764.602016    987.250587 -77021.193676 999999.999999
*  2009 11  2  0  0 20.00000000
PL15   -364.190222   6625.811136    -74.721213 999999.999999
VL15  13815.825127     65.631014 -77016.232293 999999.999999
*  2009 11  2  0  0 30.00000000
PL15   -350.350131   6625.415949   -151.730567 999999.999999
VL15  13863.820409   -855.995477 -77000.719734 999999.999999
*  2009 11  2  0  0 40.00000000
PL15   -336.463660   6624.099187   -228.719134 999999.999999
VL15  13908.581905  -1777.497047 -76974.660058 999999.999999
*  2009 11  2  0  0 50.00000000
PL15   -322.534047   6621.861041   -305.676371 999999.999999
VL15  13950.104280  -2698.741871 -76938.058807 999999.999999
*  2009 11  2  0  1  0.00000000
PL15   -308.564533   6618.701833   -382.591743 999999.999999
VL15  13988.382807  -3619.598277 -76890.923043 999999.999999
```

Clock corrections

are not provided

Excerpt of reduced-dynamic GOCE positions at begin of 2 Nov, 2009

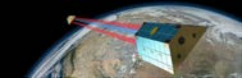

Principles of Orbit Determination

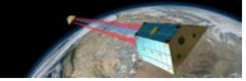

Principle of Orbit Determination

The **actual orbit** $\boldsymbol{r}(t)$ is expressed as a truncated Taylor series:

$$\boldsymbol{r}(t) = \boldsymbol{r}_0(t) + \sum_{i=1}^{n} \frac{\partial \boldsymbol{r}_0}{\partial P_i}(t) \cdot (P_i - P_{0,i})$$

$\boldsymbol{r}_0(t)$	A priori orbit
$\frac{\partial \boldsymbol{r}_0}{\partial P_i}(t)$	Partial derivative of the a priori orbit $\boldsymbol{r}_0(t)$ w.r.t. parameter P_i
$P_{0,i}$	A priori parameter values of the a priori orbit $\boldsymbol{r}_0(t)$
P_i	Parameter values of the improved orbit $\boldsymbol{r}(t)$

A **least-squares** adjustment of spacecraft tracking data yields **corrections** to the a priori parameter values $P_{0,i}$. Using the above equation, the improved (linearized) orbit $\boldsymbol{r}(t)$ may be eventually computed.

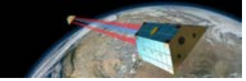

Numerical Integration (1)

Collocation algorithms (one particular class of numerical integration techniques) are subsequently used to briefly illustrate the principles of numerical integration:

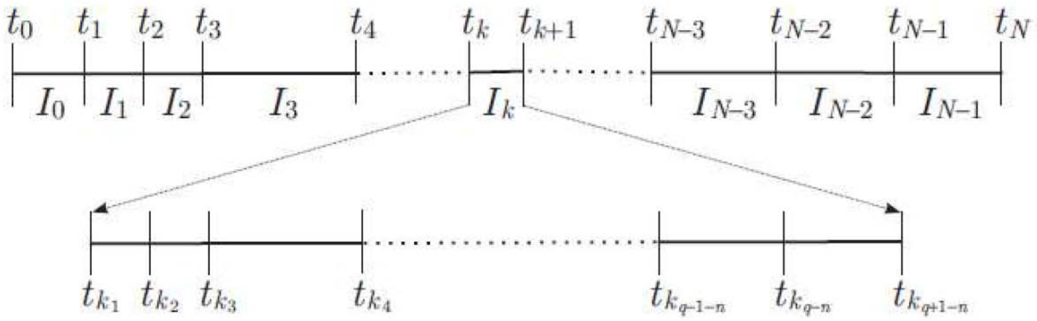
t_0
t_1
t_2
t_3
t_4
t_k
t_{k+1}
t_{N-3}
t_{N-2}
t_{N-1}
t_N
I_0
I_1
I_2
I_3
I_k
I_{N-3}
I_{N-2}
I_{N-1}
t_{k_1}
t_{k_2}
t_{k_3}
t_{k_4}
$t_{k_{q-1-n}}$
$t_{k_{q-n}}$
$t_{k_{q+1-n}}$

The original intervall is divided into N integration intervals. For each interval I_k a further subdivision is performed according to the order q of the adopted method. At these points t_{k_j} the numerical solution is requested to solve the differential equation system of order n.

(Beutler, 2005)

Numerical Integration (2)

Initial value problem in the interval I_k is given by:

$$\ddot{\mathbf{r}}_k = \mathbf{f}(t, \mathbf{r}_k, \dot{\mathbf{r}}_k)$$

with initial conditions

$$\mathbf{r}_k(t_k) \doteq \mathbf{r}_{k0} \qquad \text{and} \qquad \dot{\mathbf{r}}_k(t_k) \doteq \dot{\mathbf{r}}_{k0}$$

where the initial values are defined as

$$\mathbf{r}_{k0}^{(i)} = \begin{cases} \mathbf{r}_0^{(i)} & ;\, k = 0 \\ \mathbf{r}_{k-1}^{(i)}(t_k) & ;\, k > 0 \end{cases}$$

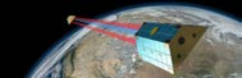

Numerical Integration (3)

The **collocation method** approximates the solution in the interval I_k by:

$$\mathbf{r}_k(t) \doteq \sum_{l=0}^{q} \frac{1}{l!}(t-t_k)^l\, \mathbf{r}_{k0}^{(l)}$$

The coefficients $\mathbf{r}_{k0}^{(l)}$, $l=0,\ldots,q$ are obtained by requesting that the numerical solution assumes the initial values and solves the differential equation system at $q-1$ different epochs t_{k_j}, $j=1,\ldots,q-1$. This leads to the conditions

$$\sum_{l=2}^{q} \frac{(t_{k_j}-t_k)^{l-2}}{(l-2)!}\,\mathbf{r}_{k0}^{(l)} = \mathbf{f}(t_{k_j},\mathbf{r}_k(t_{k_j}),\dot{\mathbf{r}}_k(t_{k_j}))\ , \quad j=1,\ldots,q-1\,.$$

They are non-linear but can be solved efficiently by an iterative procedure.

(Beutler, 2005)

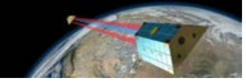

Partial Derivatives

The partial of the r -th observation w.r.t. orbit parameter P_i may be expressed as

$$\frac{\partial F_r(\boldsymbol{X})}{\partial P_i} = \left(\boldsymbol{\nabla}\left(F_r(\boldsymbol{X})\right)\right)^T \cdot \frac{\partial \boldsymbol{r}_0}{\partial P_i}(t)$$

with the gradient given by

$$\left(\boldsymbol{\nabla}\left(F_r(\boldsymbol{X})\right)\right)^T = \left(\frac{\partial F_r(\boldsymbol{X})}{\partial r_{0,1}} \; \frac{\partial F_r(\boldsymbol{X})}{\partial r_{0,2}} \; \frac{\partial F_r(\boldsymbol{X})}{\partial r_{0,3}}\right)$$

if the observations only depend on the geocentric position vector and are referring to only one epoch. The gradient only depends on the type of observations used, whereas the second term is independent of the observation type and related to the **variational equations**. This separates the observation-specific (**geometric**) part from the **dynamic** part.

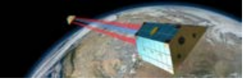

Variational Equations

For each orbit parameter P_i the corresponding **variational equation** reads as

$$\ddot{\boldsymbol{z}}_{P_i} = \boldsymbol{A}_0 \cdot \boldsymbol{z}_{P_i} + \boldsymbol{A}_1 \cdot \dot{\boldsymbol{z}}_{P_i} + \frac{\partial \boldsymbol{f}_1}{\partial P_i}$$

with $\boldsymbol{z}_{P_i}(t) \doteq \dfrac{\partial \boldsymbol{r}_0}{\partial P_i}(t)$ and the 3 x 3 matrices defined by

$$A_{0[i;k]} \doteq \frac{\partial f_i}{\partial r_{0,k}} \qquad \text{and} \qquad A_{1[i;k]} \doteq \frac{\partial f_i}{\partial \dot{r}_{0,k}}$$

f_i	i -th component of the total acceleration $\boldsymbol{f}$
$r_{0,k}$	k-th component of the geocentric position $\boldsymbol{r}_0$

For each orbit parameter P_i the **variational equation** is a linear differential equation system of second order in time. Their solutions are all needed for orbit determination.

(Jäggi, 2007)

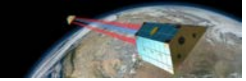

GPS-based LEO POD

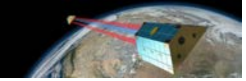

LEO Sensor Offsets

Phase center offsets $\delta \boldsymbol{r}_{leo,ant}$:

- are needed in the inertial or Earth-fixed frame and have to be transformed from the satellite frame using **attitude data** from the star-trackers

- consist of a frequency-independent **instrument offset**, e.g., defined by the center of the instrument‘s mounting plane (CMP) in the satellite frame

- consist of frequency-dependent **phase center offsets** (PCOs), e.g., defined wrt the center of the instrument‘s mounting plane in the antenna frame (ARF)

- consist of frequency-dependent **phase center variations** (PCVs) varying with the direction of the incoming signal, e.g., defined wrt the PCOs in the antenna frame

Example: GOCE Sensor Offsets (1)

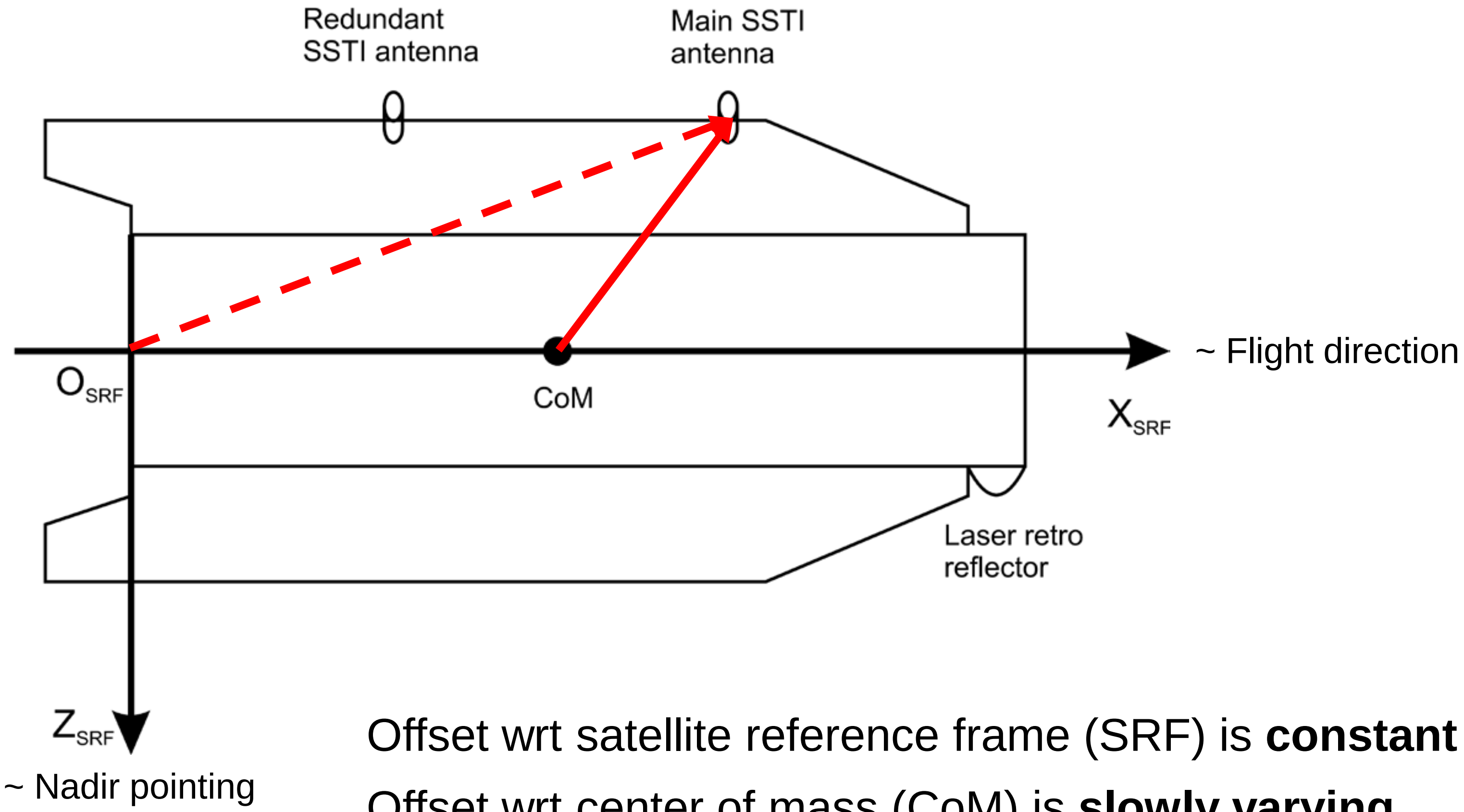
Redundant SSTI antenna
Main SSTI antenna
~ Flight direction
O_{SRF}
CoM
X_{SRF}
Laser retro reflector
Z_{SRF}
~ Nadir pointing

Offset wrt satellite reference frame (SRF) is **constant**

Offset wrt center of mass (CoM) is **slowly varying**

Example: GOCE Sensor Offsets (2)

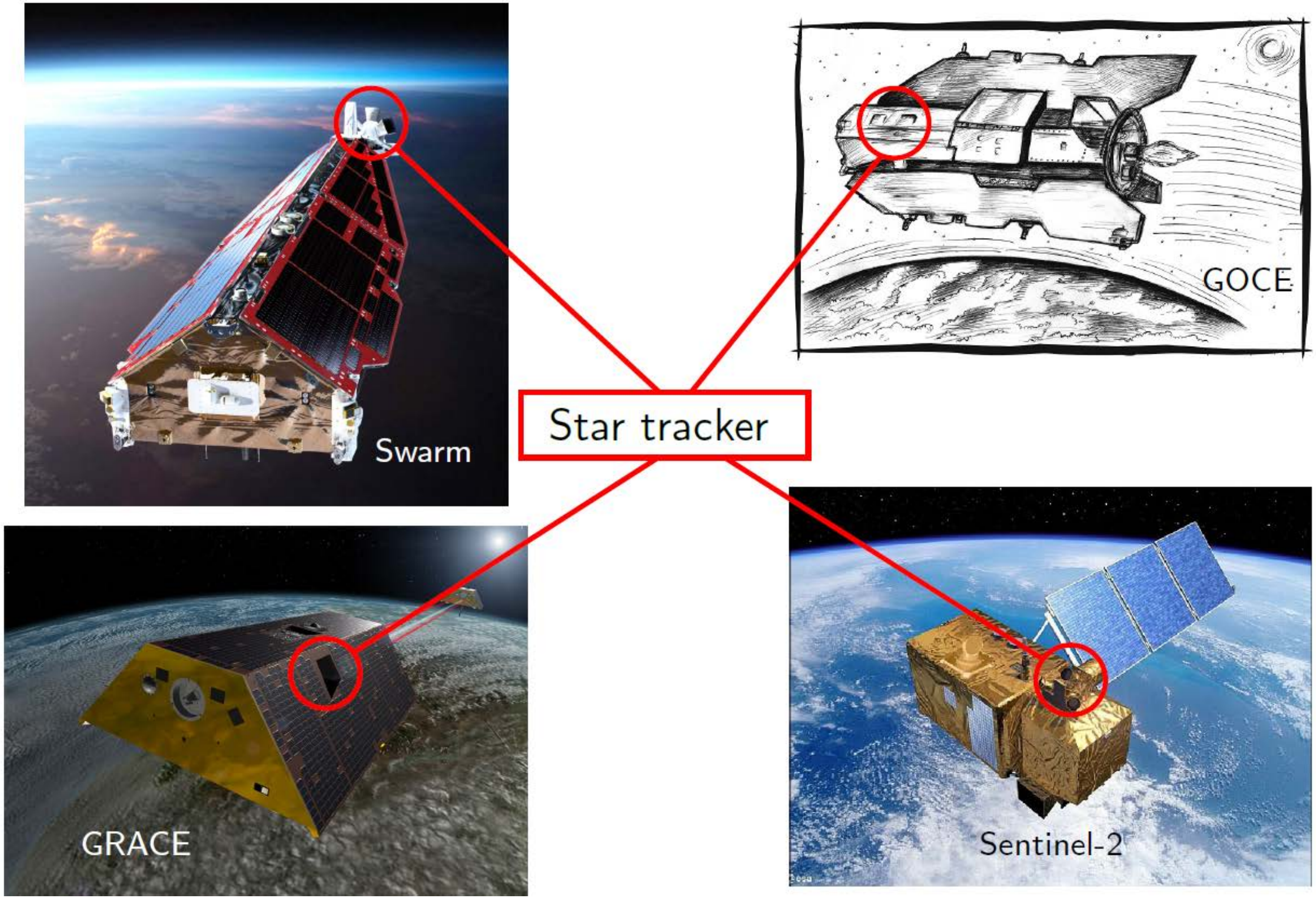

Star tracker

Swarm
GOCE
GRACE
Sentinel-2

Spaceborne GPS Antennas: GOCE

L1, L2, Lc phase center offsets

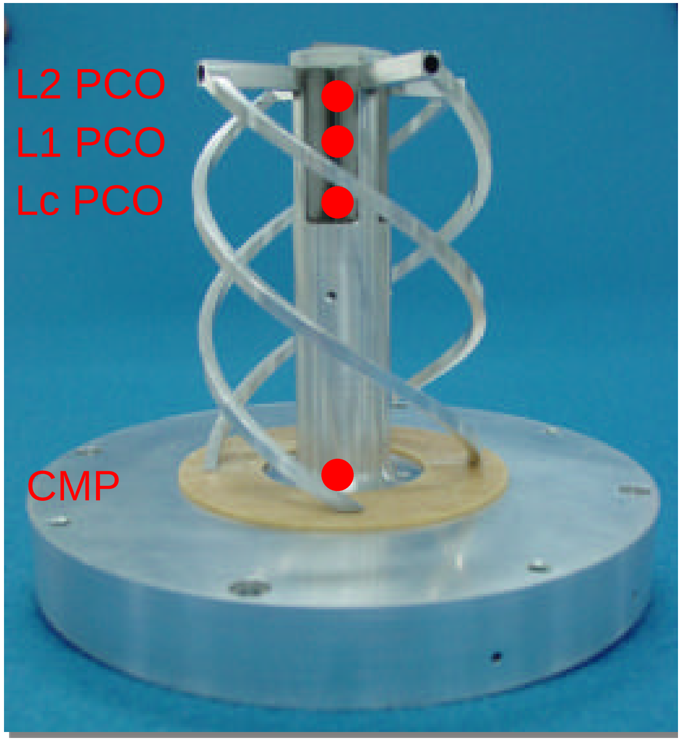

Measured from ground calibration in anechoic chamber

Lc phase center variations

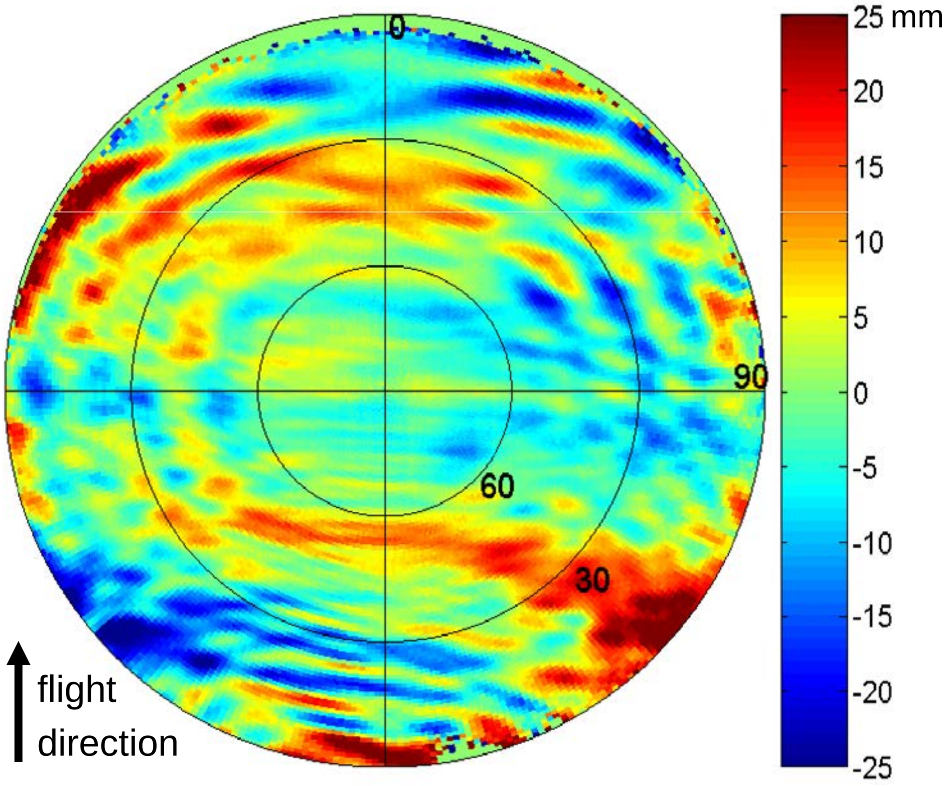

Empirically derived during orbit determination according to Jäggi et al. (2009)

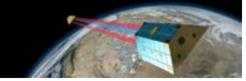

Spaceborne GPS Antennas: Swarm

Swarm GPS antenna

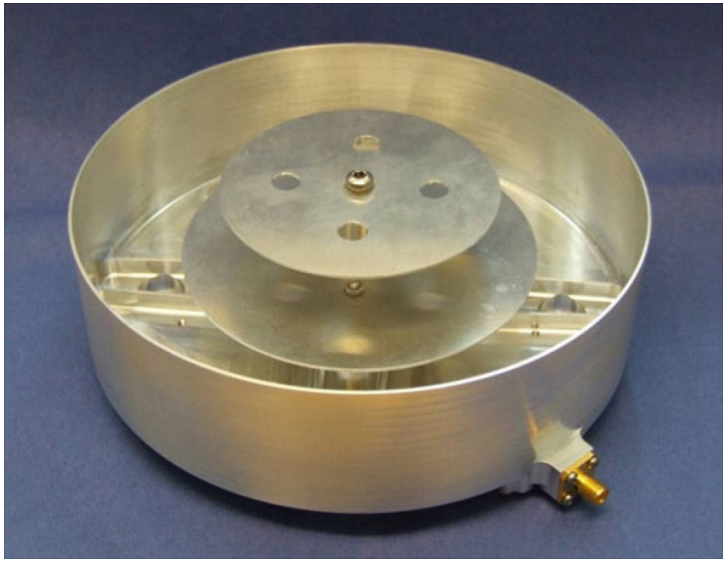

Multipath shall be minimzed by chokering

Lc phase center variations

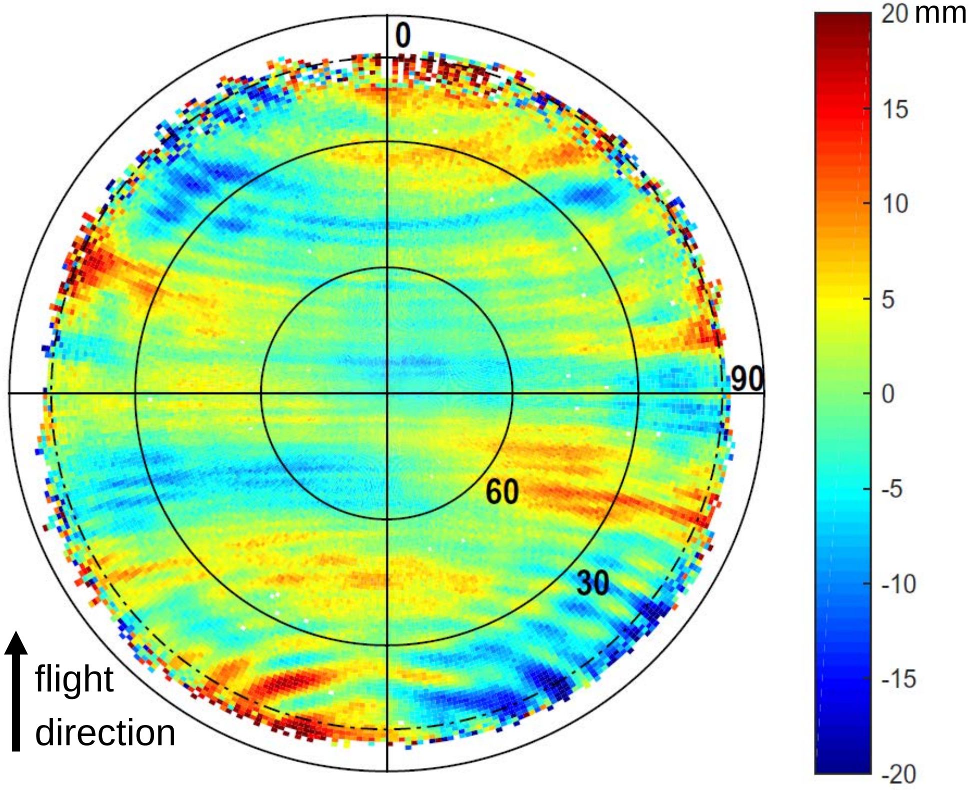

Empirically derived during orbit determination according to Jäggi et al. (2016)

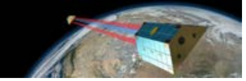

Spaceborne GPS Antennas: GRACE

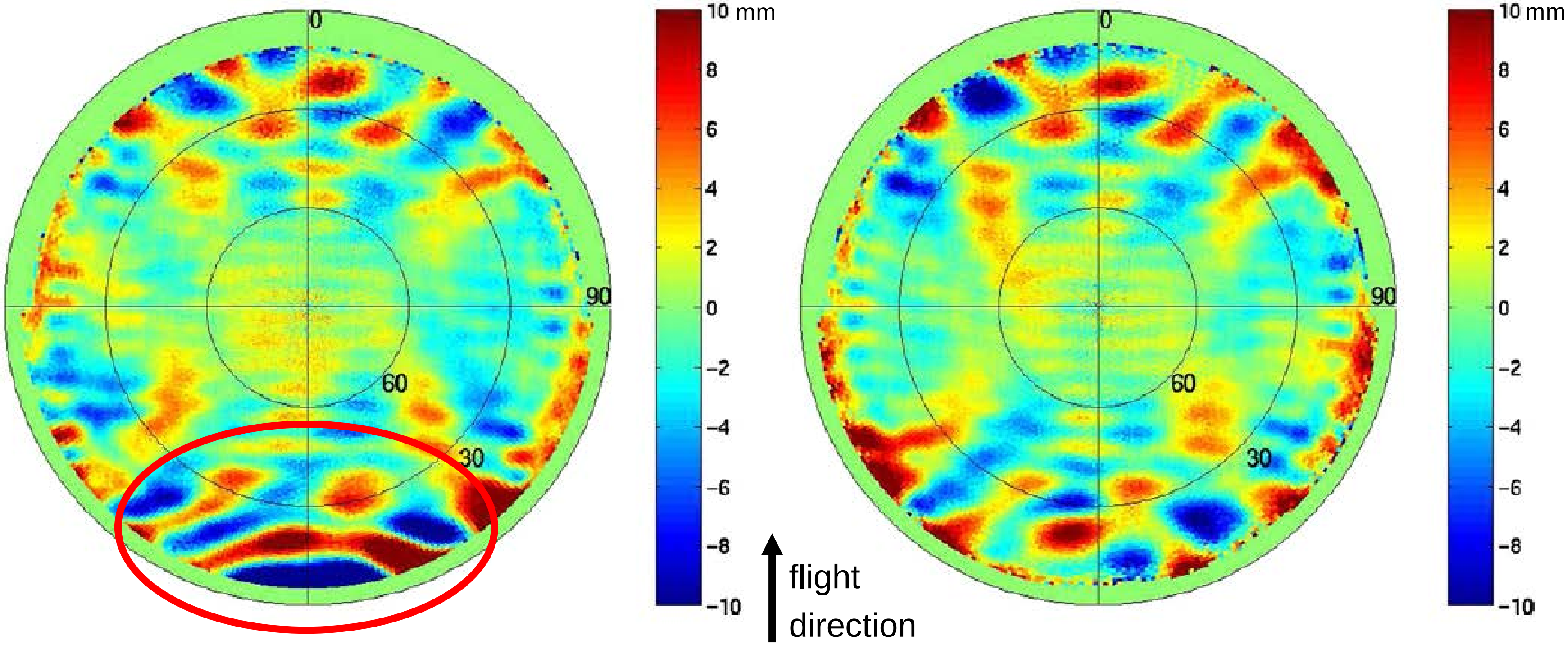

GRACE-A
(occultation antenna switched on)

GRACE-B

(Jäggi et al., 2009)

Visualization of Orbit Solutions

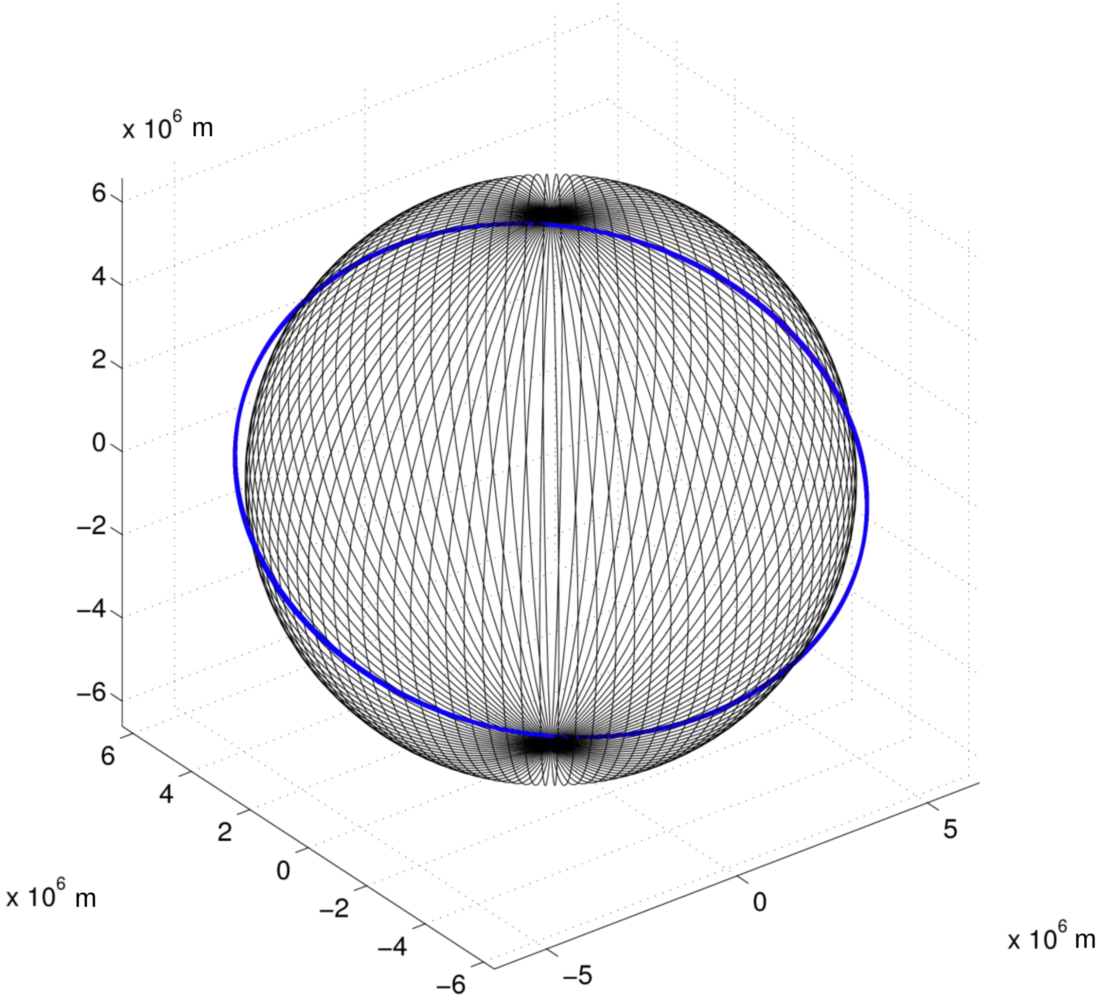

It is more instructive to look at differences between orbits in well suited coordinate systems …

Co-Rotating Orbital Frames

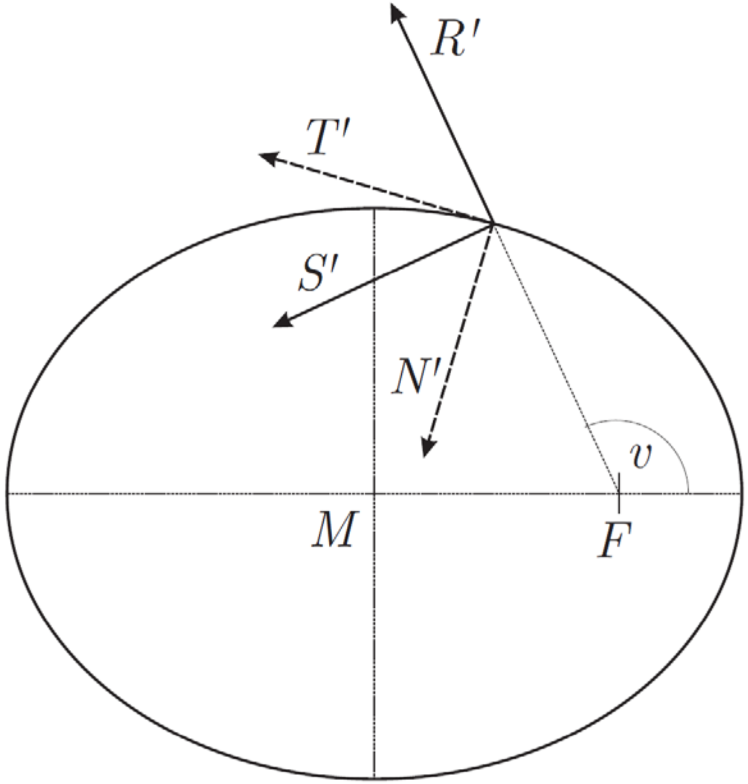

R, S, C unit vectors are pointing:

- into the radial direction
- normal to **R** in the orbital plane
- normal to the orbital plane (cross-track)

T, N, C unit vectors are pointing:

- into the tangential (along-track) direction
- normal to **T** in the orbital plane
- normal to the orbital plane (cross-track)

Small eccentricities: **S**~**T** (velocity direction)

Orbit Differences KIN-RD (Sentinel-3A)

Differences at epochs of kin. positions

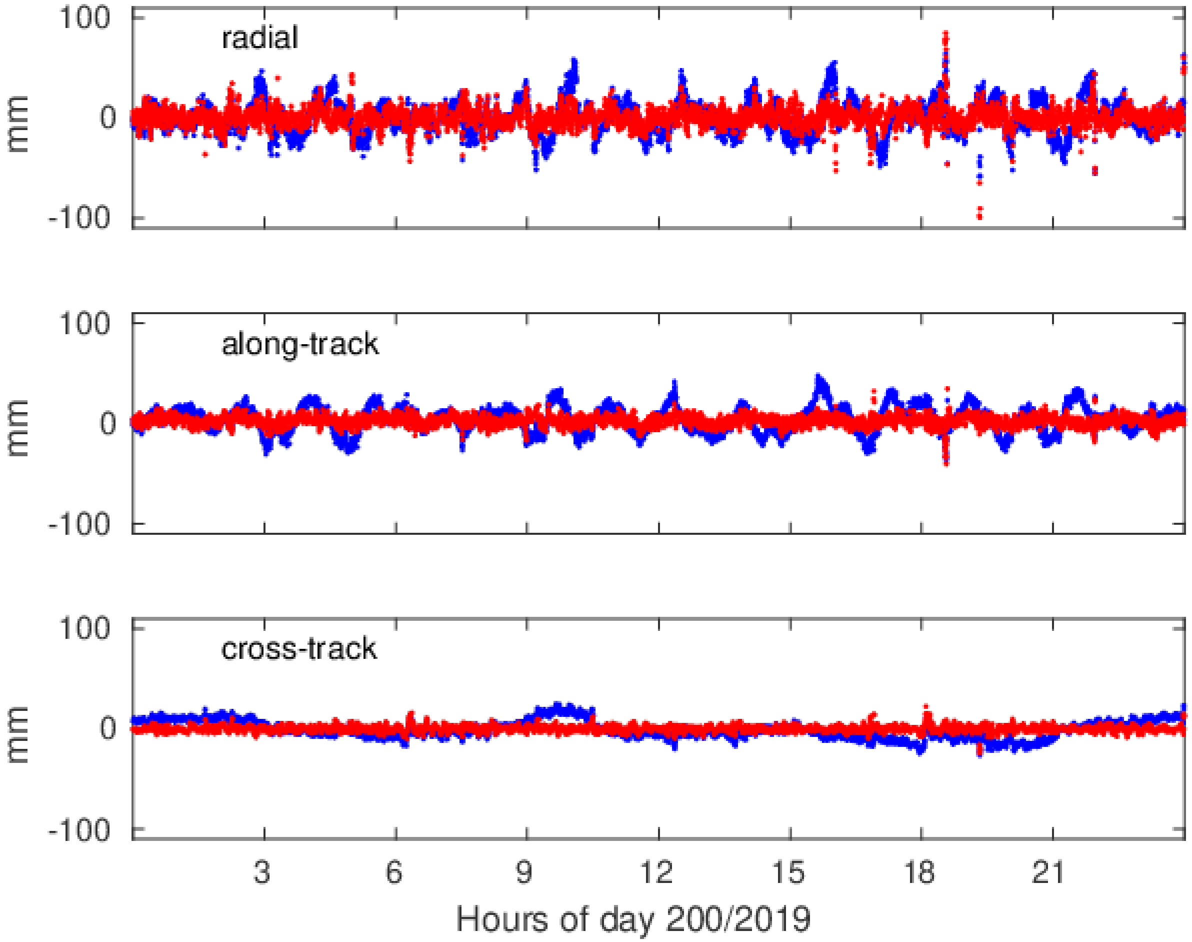

Comparison of ambiguity-float solutions and ambiguity-fixed solutions.

Orbit Differences KIN-RD (COSMIC-2)

Differences at epochs of kin. positions, FM-1, POD-1

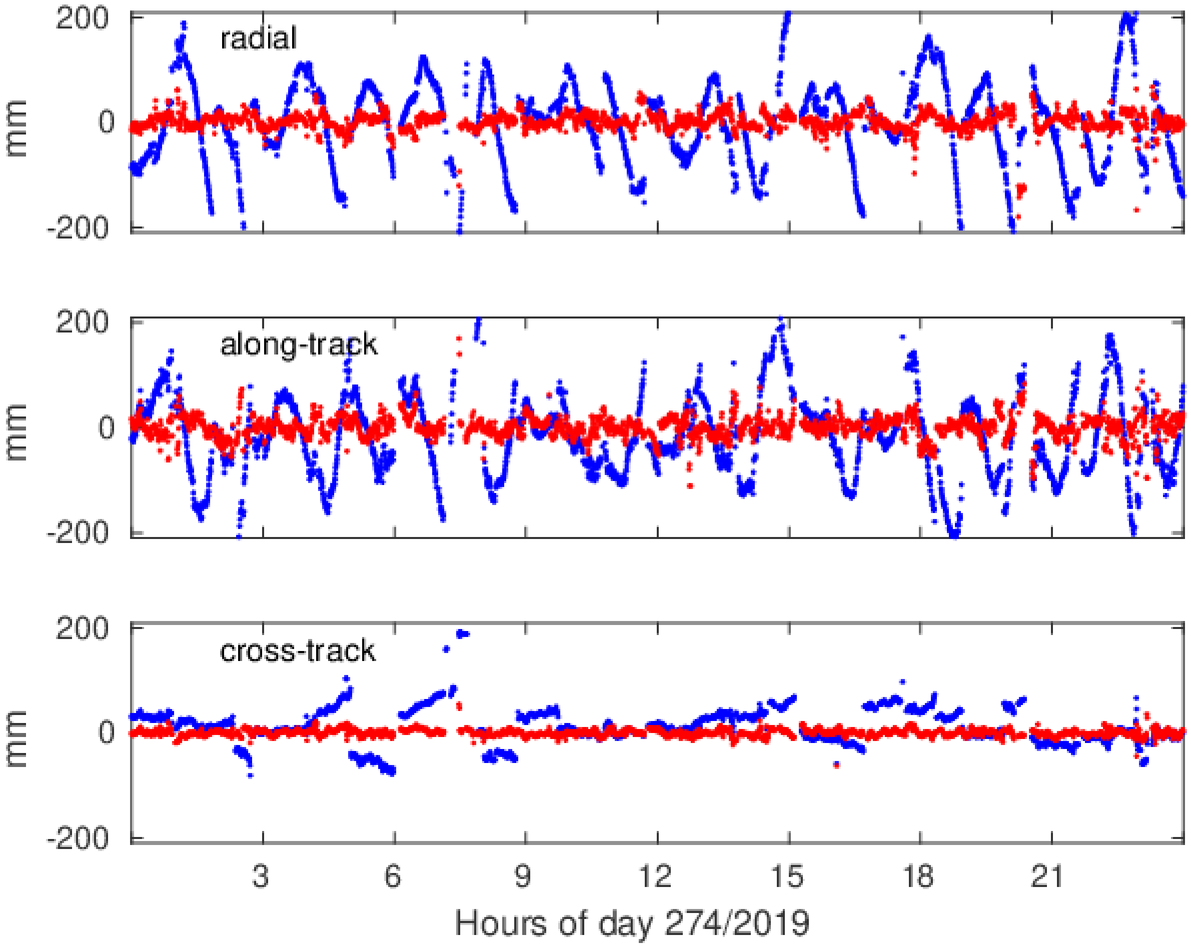

Comparison of ambiguity-float solutions and ambiguity-fixed solutions. (Jäggi et al. 2021)

Orbit Differences KIN-RD (GOCE)

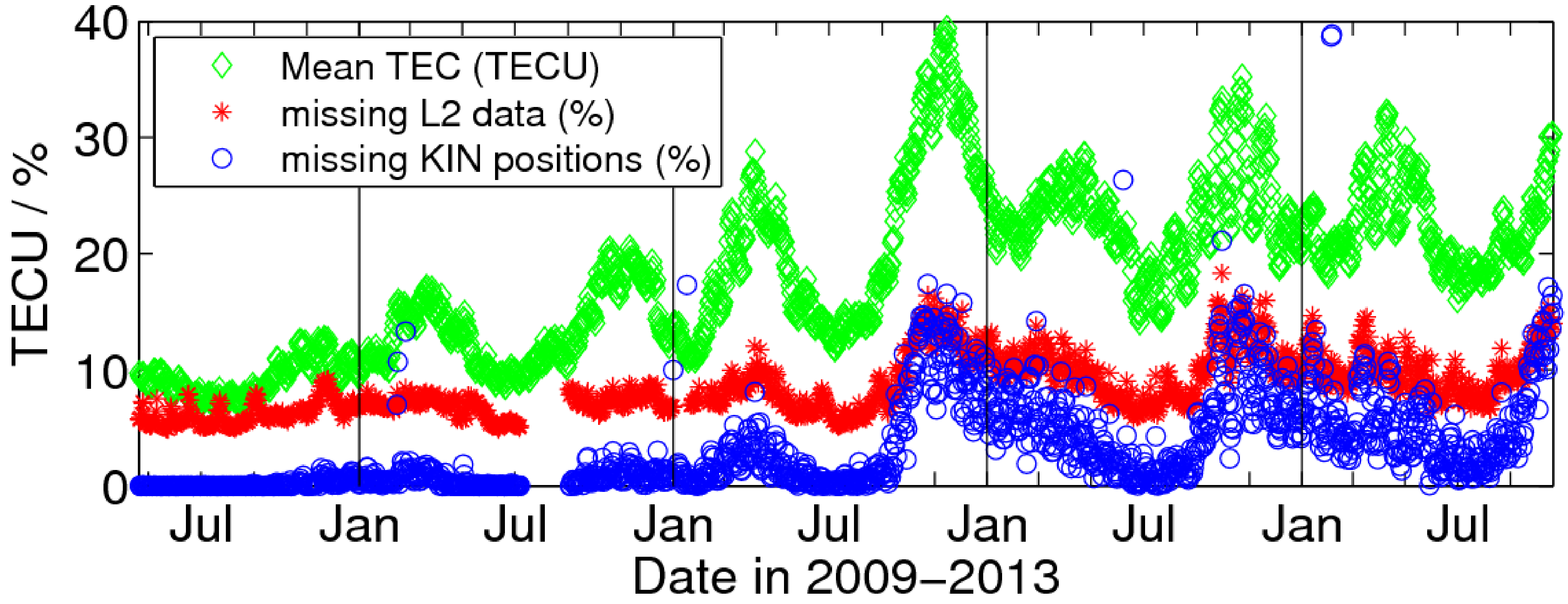

The result illustrates the **consistency** between both orbit-types. The level of the differences is usually given by the quality of the kinematic positions.

The differences are highly correlated with the **ionosphere activity** and with **data losses on L2**.

(Bock et al., 2014)

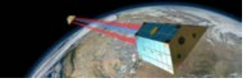

RMS of Carrier Phase Residuals (Sentinel-1)

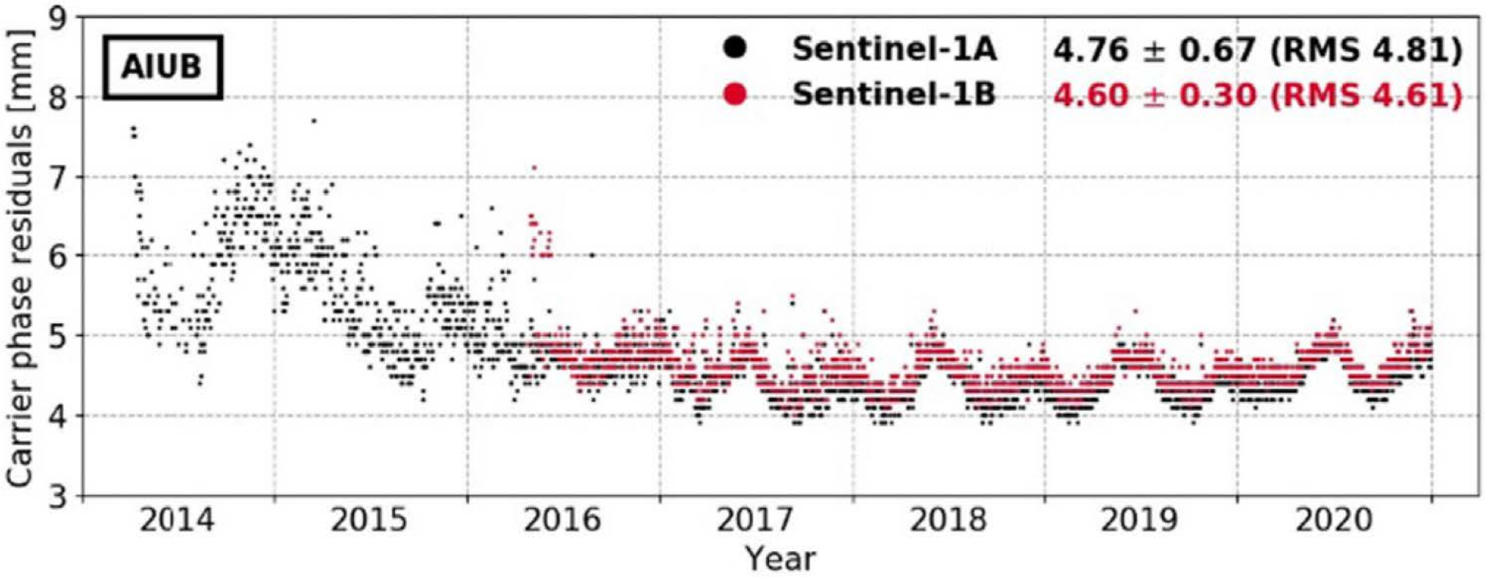

The plot illustrates the **quality** of the orbit fit. The level is given by the adopted parametrization, depending on how dynamic the orbit parametrization is.

The variations reveal again the impact of the **ionosphere activity** and also further **modeling deficiencies.**

(Fernández et al., 2022)

Consequences of Ionospheric Effects in Orbits

For GOCE systematic effects around the geomagnetic equator were observed in the ionosphere-free GPS phase residuals **=> affects kinematic positions**

Degradation of kinematic positions around the geomagnetic equator propagates into gravity field solutions.

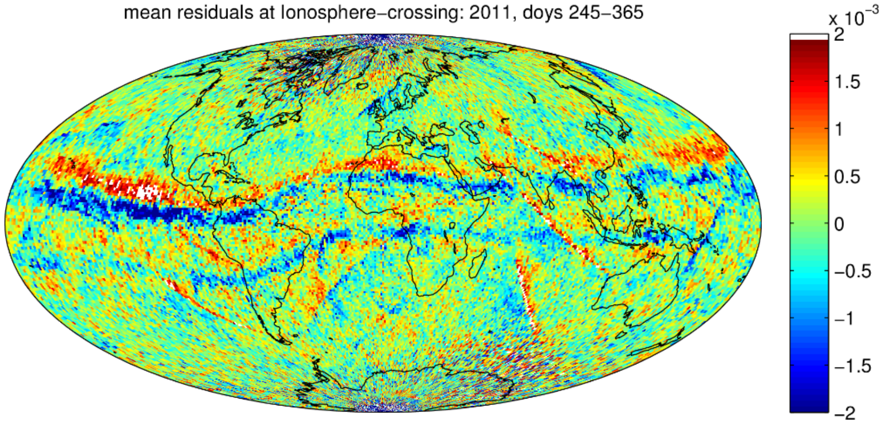
mean residuals at Ionosphere−crossing: 2011, doys 245−365
x 10^{-3}
2
1.5
1
0.5
0
−0.5
−1
−1.5
−2

Phase observation residuals (- 2 mm … +2 mm) mapped to the ionosphere piercing point

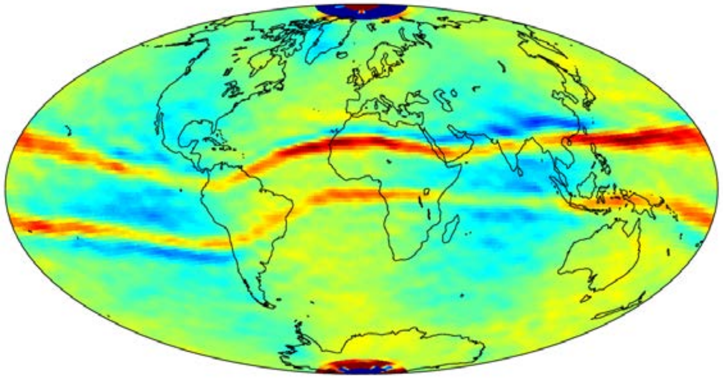

Geoid height differences
(−5 cm … 5 cm);
R4 period

(Jäggi et al., 2015)

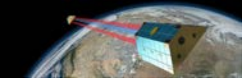

Systematic Errors in GPS Data (1)

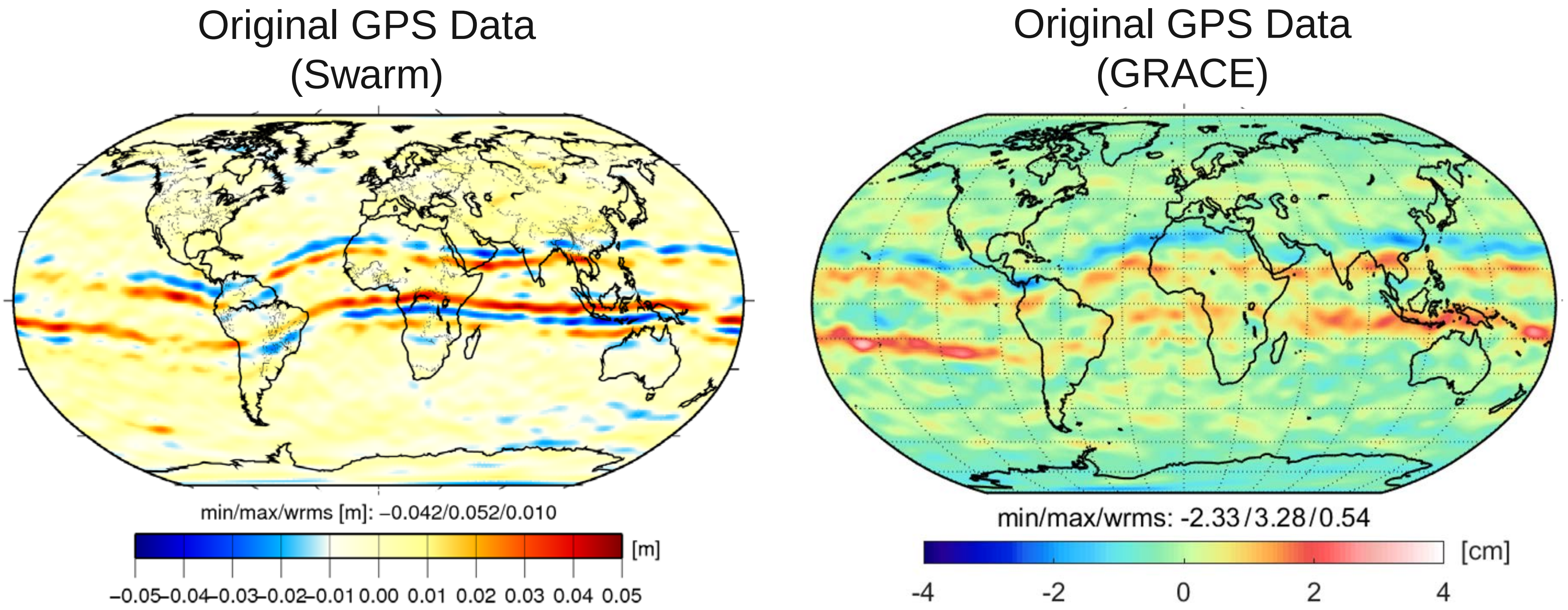

Original GPS Data (Swarm)

Original GPS Data (GRACE)

min/max/wrms [m]: −0.042/0.052/0.010
[m]
−0.05 −0.04 −0.03 −0.02 −0.01 0.00 0.01 0.02 0.03 0.04 0.05
min/max/wrms: -2.33 / 3.28 / 0.54
[cm]
-4 -2 0 2 4

(Differences wrt GOCO05S, 400 km Gauss smoothing adopted)

Systematic signatures along the geomagnetic equator are **"not"** visible when using original L1B RINEX GPS data files from the GRACE mission.

(Jäggi et al., 2016)

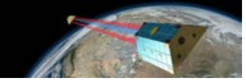

Systematic Errors in GPS Data (2)

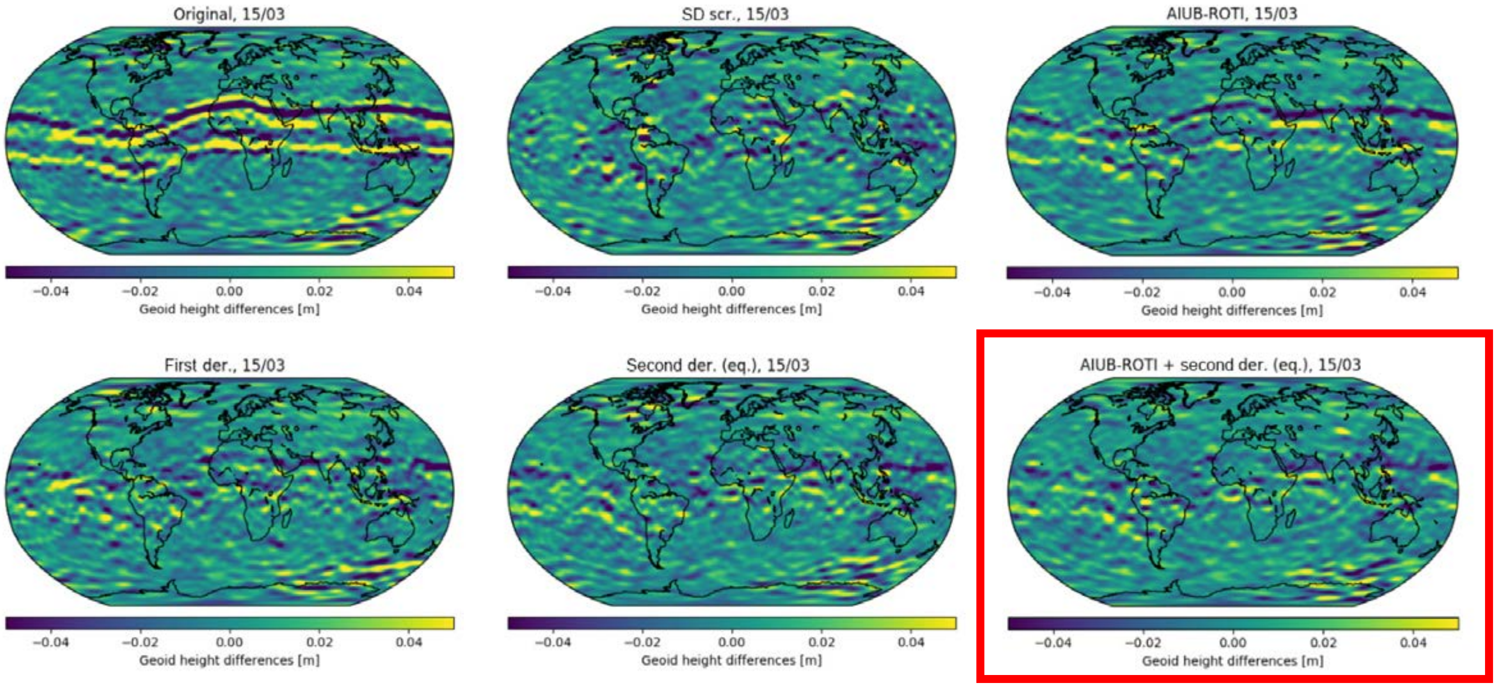
Original, 15/03
SD scr., 15/03
AIUB-ROTI, 15/03
First der., 15/03
Second der. (eq.), 15/03
AIUB-ROTI + second der. (eq.), 15/03
−0.04
−0.02
0.00
0.02
0.04
Geoid height differences [m]

(Differences wrt JPL-GRACE-RL06, 400 km Gauss smoothing adopted)

Systematic signatures along the geomagnetic equator may be efficiently reduced when down-weighting the GPS data using derivatives of the geometry-free linear combination. ROTI-based down-weighting additionally reduces scintillation noise.

(Schreiter et al., 2019)

Sensitivity to the Time-Variable Gravity Field Model (1)

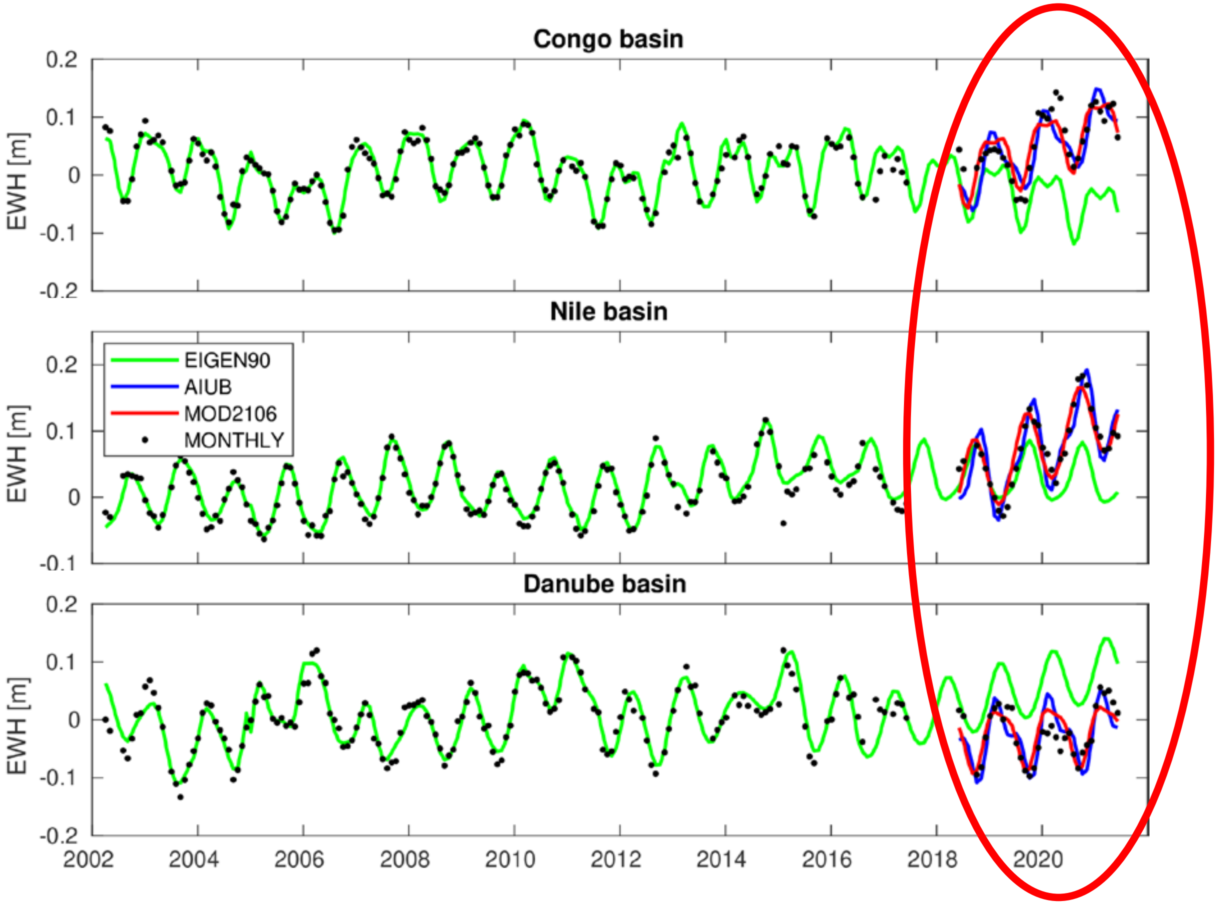

The predictions of the EIGEN-GRGS.RL04 model (containing no data after 2017) are rather poor as shown here for three river basins. The new fitted signal model (FSM) to COST-G monthly solutions has clear advantages.

(Peter et al., 2022)

Sensitivity to the Time-Variable Gravity Field Model (2)

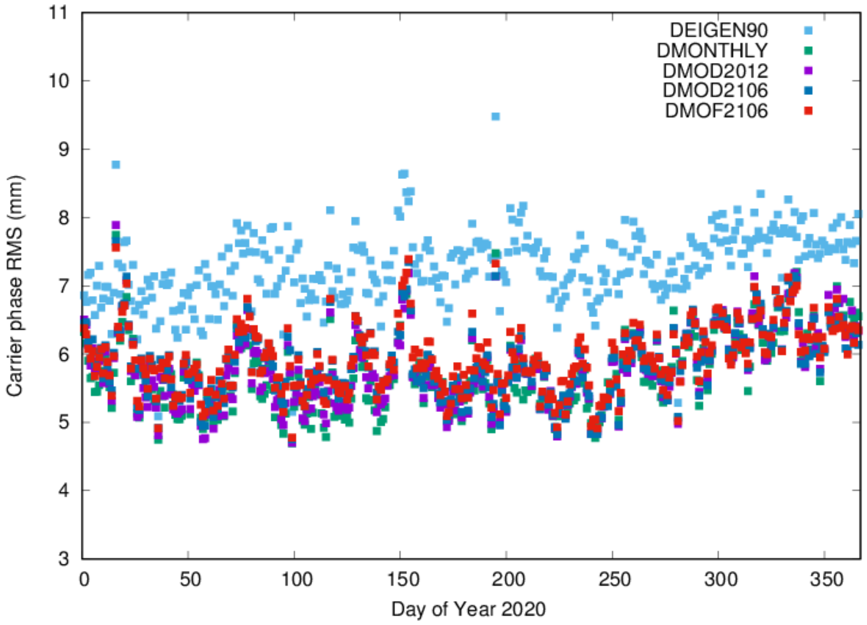

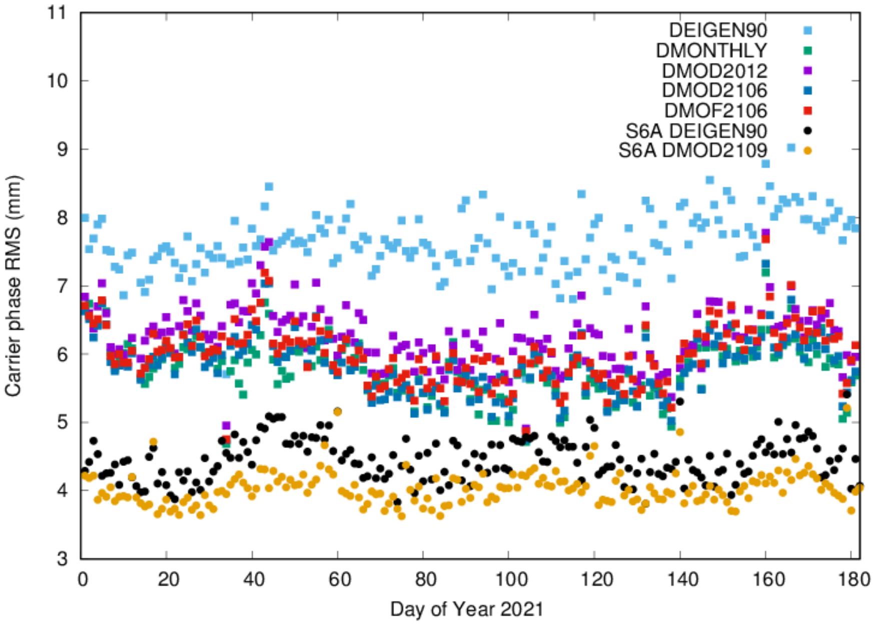

Monthly COST-G GRACE-FO gravity fields (🟩) outperform GRACE-based static fields (🟦) with co-estimated time-variations for Sentinel-3B (left and right plot).

COST-G fitted signal models (FSM) perform comparably good (🟪 🟦 🟥, left plot), which also holds for Sentinel-6A (🟡, right plot). In particular the COST-G FSM show also good prediction capabilities (🟪, right plot).

(Peter et al., 2022)

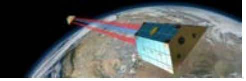

Orbit Validation

Orbit Comparisons (Spire FM099)

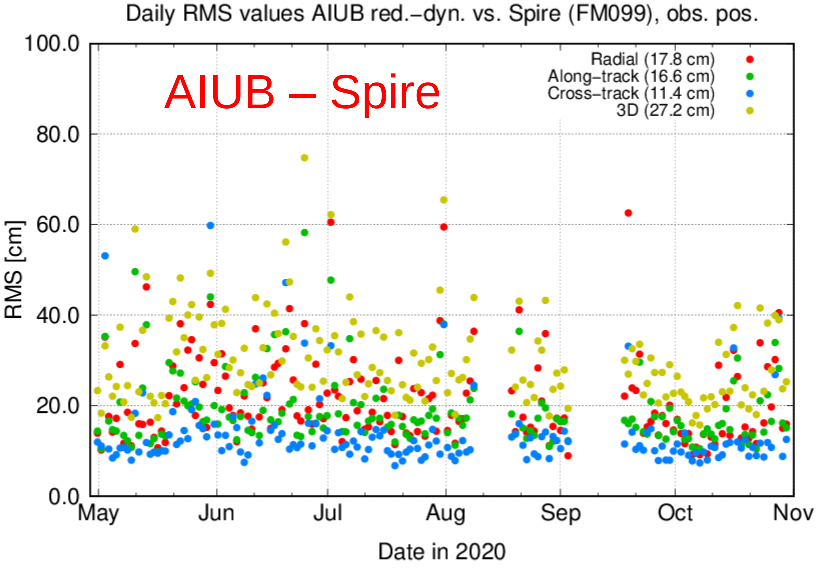

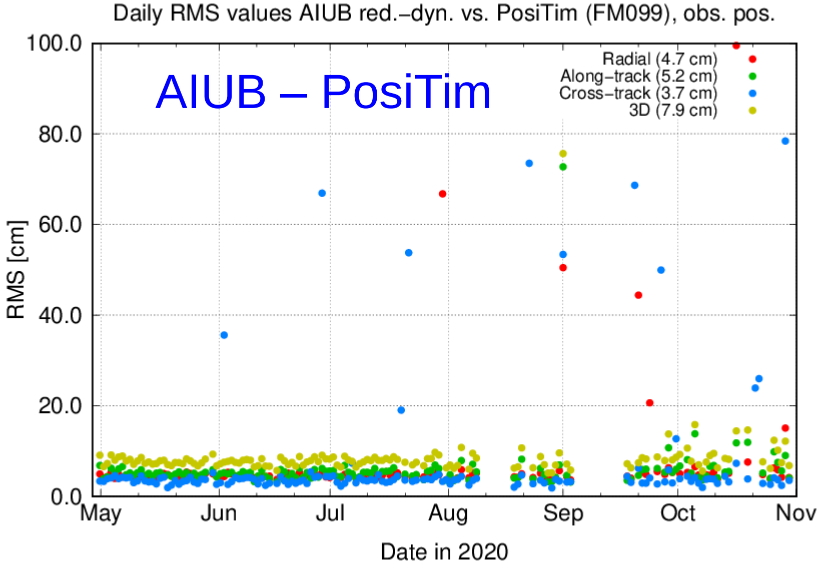

Orbit comparisons between solutions computed **with different software packages** are helpful, especially if no external orbit validations are possible.

The plots show for the example of one Spire satellite that orbit differences AIUB – PosiTim are significantly smaller than the orbit differences AIUB – Spire.

(Jäggi et al., 2022)

GRACE Orbit Validation with K-Band

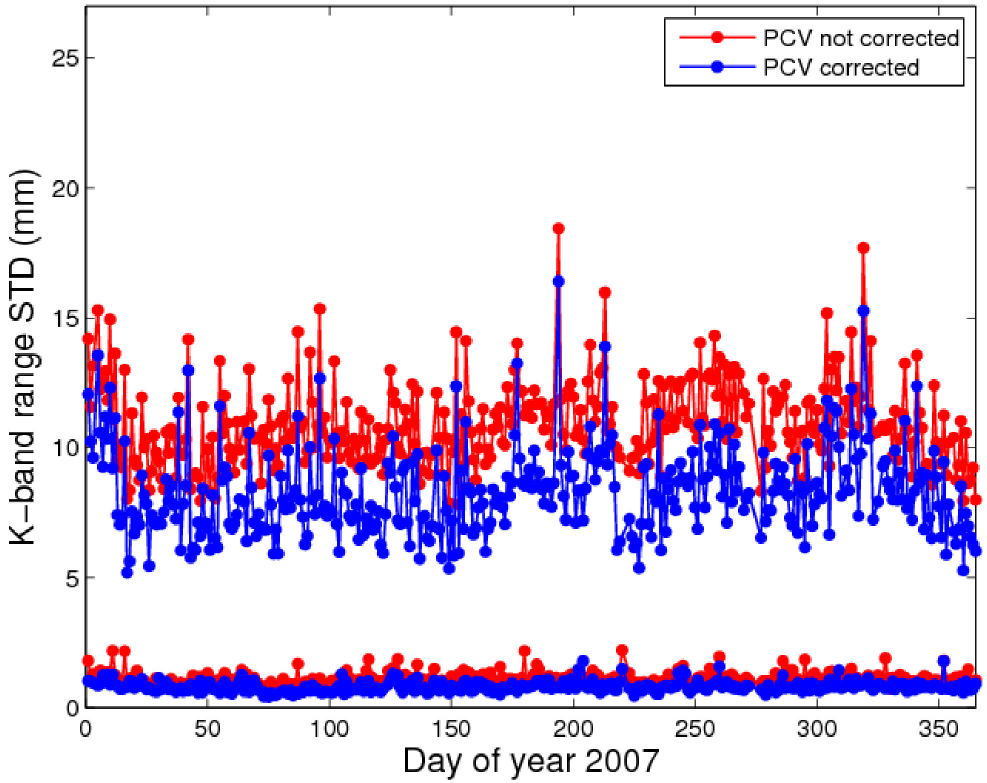

ZD solution
< 1cm

DD solution
(ambiguity-fixed)
< 1mm

The ultra-precise and continuously available K-Band data allow it to validate the **inter-satellite distances** between the GRACE satellites. Thanks to this validation, e.g., PCV maps were recognized to be crucial for high-quality POD.

(Jäggi et al., 2009)

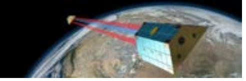

Orbit Validation with SLR (GOCE)

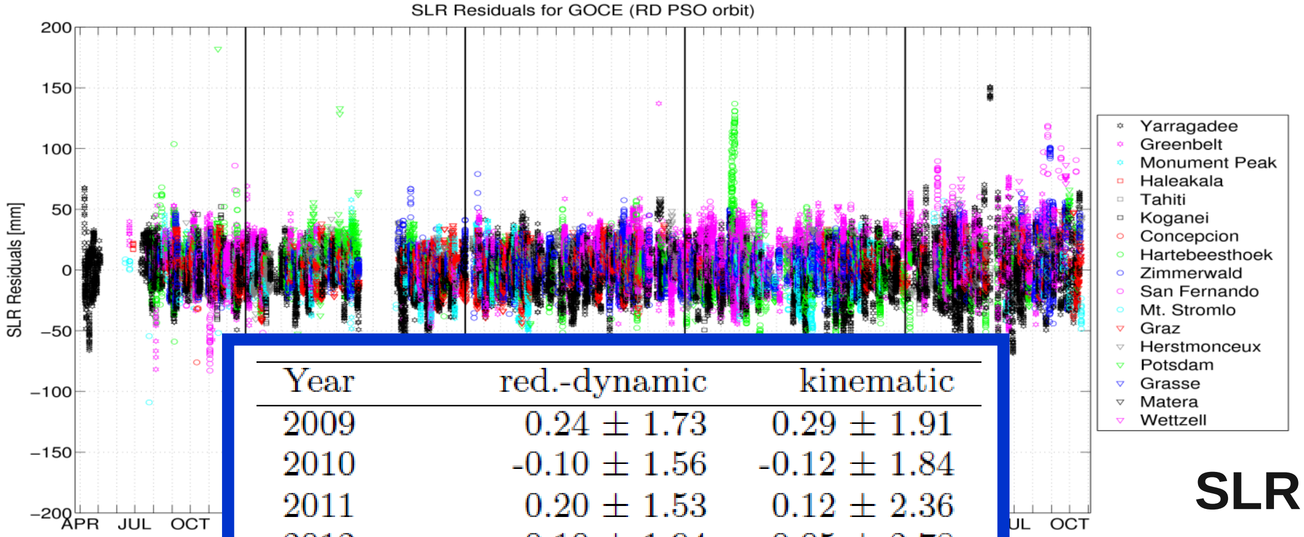

Reduced-dynamic

Year	red.-dynamic	kinematic
2009	0.24 ± 1.73	0.29 ± 1.91
2010	-0.10 ± 1.56	-0.12 ± 1.84
2011	0.20 ± 1.53	0.12 ± 2.36
2012	0.10 ± 1.94	-0.05 ± 2.78
2013	0.63 ± 2.62	0.45 ± 3.17
2009–2013	0.18 ± 1.84	0.10 ± 2.42

SLR statistics:

Mean ± RMS (cm)

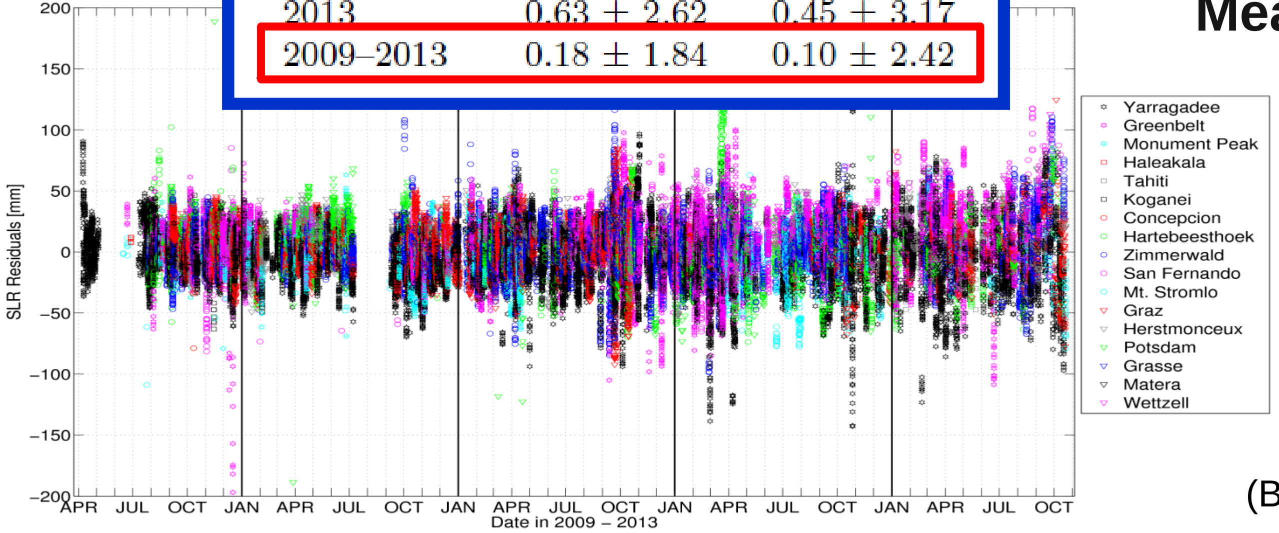

Kinematic

(Bock et al., 2014)

Impact of Undifferenced Ambiguity Resolution (1)

SLR Validation of Sentinel-3A

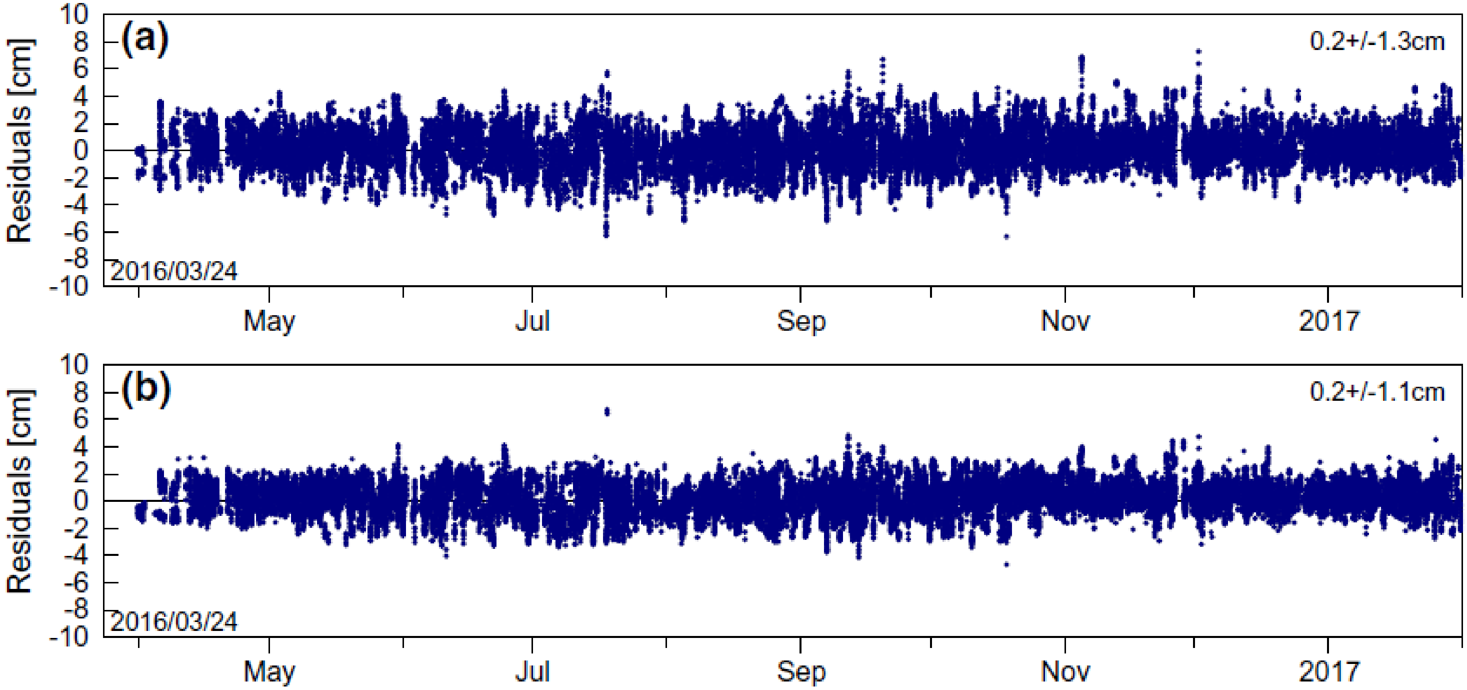

Single-receiver ambiguity fixing may be enabled by using phase bias products and corresponding clock products provided by the IGS analysis centers without the need to form any baselines. It allows to identify lateral offsets in the GPS antenna or center-of-mass location and to significantly stabilize the LEO trajectories.

(Montenbruck et al., 2018)

Impact of Undifferenced Ambiguity Resolution (2)

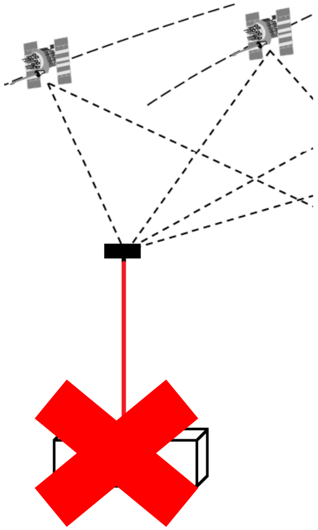

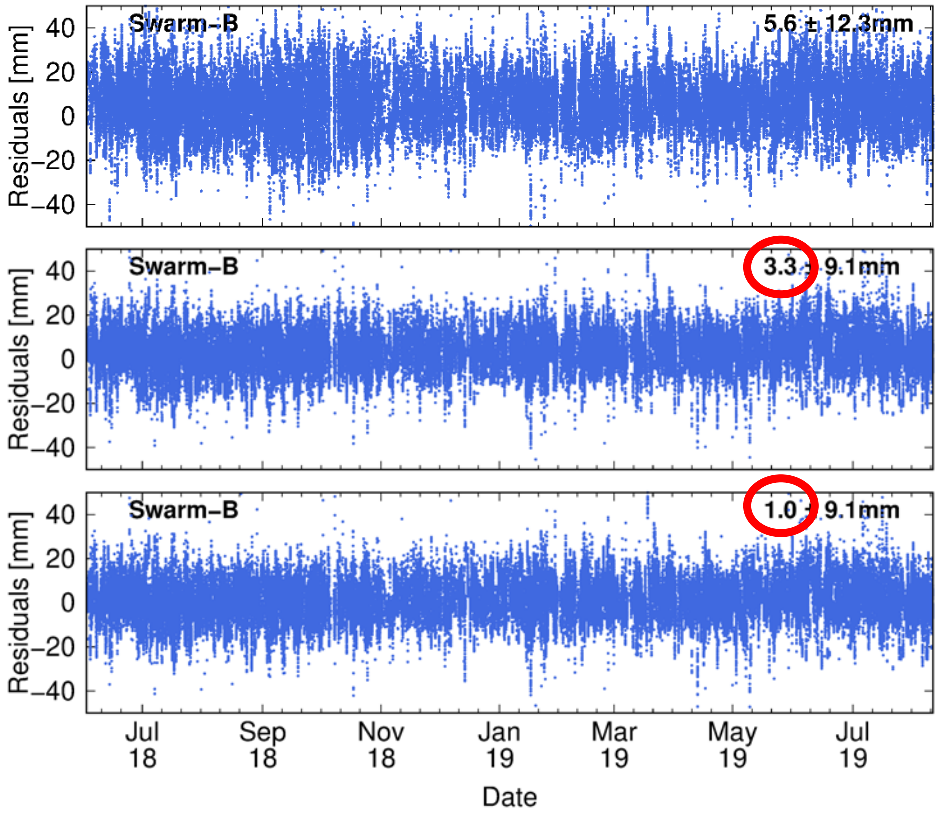

Ambiguity-float, no non-grav. modeling

Ambiguity-fixed, no non-grav. modeling

Ambiguity-fixed, with non-grav. modeling

LEO POD significantly profits from single-receiver ambiguity fixing techniques and high-quality signal-specific phase bias products, e.g., by Schaer et al. (2021).

(Arnold et al., 2019; Mao et al., 2021)

Multi-GNSS LEO POD

SLR Validation of Sentinel-6A

Station offsets adjusted

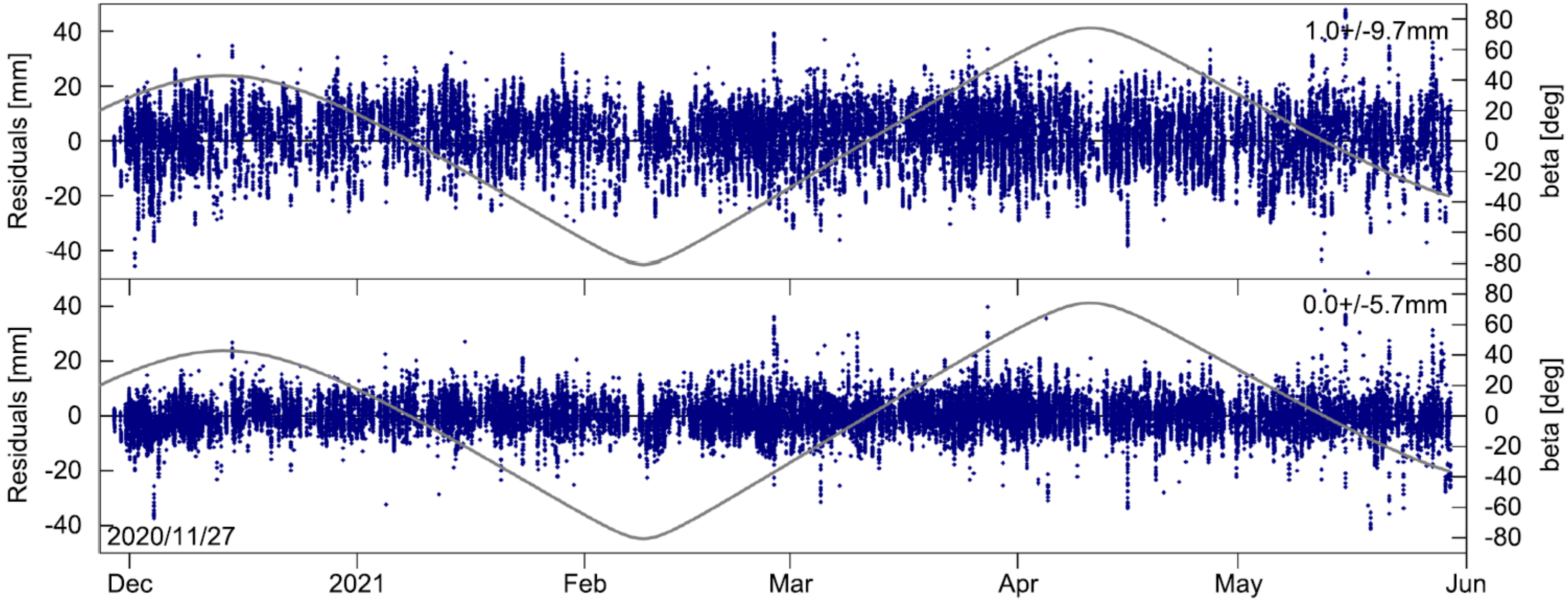

While **Galileo** measurements **exhibit 30–50% smaller RMS errors** than those of GPS, the POD benefits most from the availability of an increased number of satellites. For Sentinel-6A a 1-cm consistency of ambiguity-fixed GPS-only and Galileo-only solutions with the dual-constellation orbits can be demonstrated.

(Montenbruck et al., 2021)

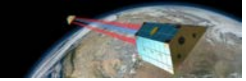

Literature (1)

Arnold, D., A. Jäggi, S. Schaer, C. Kobel, U. Meyer, L. Geisser, O. Montenbruck (2019): Performance of dynamic and ambiguity-fixed LEO orbits in SLR validation and network calibration. OSTST 2019 Meeting, October 21-25, 2019.

Beutler, G. (2005) Methods of Celestial Mechanics. Vol 1: Physical, Mathematical, and Numerical Principles. Springer, ISBN 3-540-40749-9

Blewitt, G. (1997): Basics of the GPS Technique: Observation Equations, in *Geodetic Applications of GPS*, Swedish Land Survey, pp. 10-54, available at http://www.sbg.ac.at/mat/staff/revers/lectures/2006_2007/GPS/GPSBasics.pdf

Bock, H., R. Dach, A. Jäggi, G. Beutler (2009): High-rate GPS clock corrections from CODE: Support of 1 Hz applications. *Journal of Geodesy*, 83(11), 1083-1094, doi: 10.1007/s00190-009-0326-1

Bock, H., A. Jäggi, G. Beutler, U. Meyer (2014): GOCE: Precise orbit determination for the entire mission. *Journal of Geodesy*, 88(11), 1047-1060, doi: 10.1007/s00190-014-0742-8

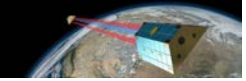

Literature (2)

Dach, R., E. Brockmann, S. Schaer, G. Beutler, M. Meindl, L. Prange, H. Bock, A. Jäggi, L. Ostini (2009): GNSS processing at CODE: status report, *Journal of Geodesy*, 83(3-4), 353-366, doi: 10.1007/s00190-008-0281-2

Fernández, M., H. Peter, D. Arnold, B. Duan, W. Simons, M. Wermuth, S. Hackel, J. Fernández, A. Jäggi, U. Hugentobler, P. Visser, P. Féménias (2022): Copernicus Sentinel–1 POD Reprocessing Campaign. *Advances in Space Research*, 70(2), 249-267, doi: 10.1016/j.asr.2022.04.036

Grombein, T., M. Lasser, D. Arnold, U. Meyer, A. Jäggi (2022): Determination and Combination of Monthly Gravity Field Time Series from Kinematic Orbits of GRACE, GRACE-FO and Swarm. *IAG Symposia Series,* in press, doi: 10.1007/1345_2022_163

Jäggi, A., U. Hugentobler, G. Beutler (2006): Pseudo-stochastic orbit modeling techniques for low-Earth satellites. *Journal of Geodesy*, 80(1), 47-60, doi: 10.1007/s00190-006-0029-9

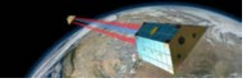

Literature (3)

Jäggi, A. (2007): Pseudo-Stochastic Orbit Modeling of Low Earth Satellites Using the Global Positioning System. *Geodätisch-geophysikalische Arbeiten in der Schweiz*, 73, Schweizerische Geodätische Kommission, available at http://www.sgc.ethz.ch/sgc-volumes/sgk-73.pdf

Jäggi, A., R. Dach, O. Montenbruck, U. Hugentobler, H. Bock, G. Beutler (2009): Phase center modeling for LEO GPS receiver antennas and its impact on precise orbit determination. *Journal of Geodesy*, 83(12), 1145-1162, doi: 10.1007/s00190-009-0333-2

Jäggi, A., L. Prange, U. Hugentobler (2011): Impact of covariance information of kinematic positions on orbit reconstruction and gravity field recovery. *Advances in Space Research*, 47(9), 1472-1479, doi: 10.1016/j.asr.2010.12.009

Jäggi, A., H. Bock, U. Meyer, G. Beutler, J. van den IJssel (2015): GOCE: assessment of GPS-only gravity field determination. *Journal of Geodesy*, 89(1), 33-48. doi: 10.1007/s00190-014-0759-z

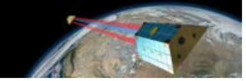

Literature (4)

Jäggi, A., C. Dahle, D. Arnold, H. Bock, U. Meyer, G. Beutler, J. van den IJssel (2016): Swarm kinematic orbits and gravity fields from 18 months of GPS data. *Advances in Space Research*, 57(1), 218-233, doi: 10.1016/j.asr.2015.10.035

Jäggi, A., C. Dahle, D. Arnold, H. Bock, U. Meyer, G. Beutler, J. van den IJssel (2016): Swarm kinematic orbits and gravity fields from 18 months of GPS data. *Advances in Space Research*, 57(1), 218-233, doi: 10.1016/j.asr.2015.10.035

Jäggi, A., D. Arnold, J. Weiss, D. Hunt (2021): Assessment of COSMIC-2 reduced-dynamic and kinematic orbit determination, vEGU21: Gather Online, 19-30 April, 2021

Jäggi, A., H. Peter, D. Arnold, X. Mao (2022): Precise Orbit Determination of the Spire Satellite Constellation for Geodetic, Geophysical, and Ionospheric Applications – Project Overview and First Orbit Determination Results. COSPAR 2022 44th Scientific Assembly, Athens, Greece, 16-24 July, 2022

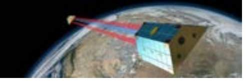

Literature (5)

Lasser, M., U. Meyer, A. Jäggi, T. Mayer-Gürr, A. Kvas, K.H. Neumayer, C. Dahle, F. Flechtner, J.-M. Lemoine, I. Koch, M. Weigelt, J. Flury (2020): Benchmark data for verifying background model implementations in orbit and gravity field determination software. *Advances in Geosciences*, 55, 1-11, doi: 10.5194/adgeo-55-1-2020

Mao, X., D. Arnold, V. Girardin, A. Villiger, A. Jäggi (2021): Dynamic GPS-based LEO orbit determination with 1 cm precision using the Bernese GNSS Software. *Advances in Space Research*, 67(2), 788-805, doi: 10.1016/j.asr.2020.10.012

Mayer-Gürr, T., A. Kvas (2019): COST-G software comparison, Graz University of Technology, benchmark data set available at: ftp://ftp.tugraz.at/outgoing/ITSG/COST-G/softwareComparison/

Montenbruck, O., S. Hackel, A. Jäggi (2018): Precise orbit determination of the Sentinel-3A altimetry satellite using ambiguity-fixed GPS carrier phase observations. *Journal of Geodesy*, 92(7), 711-726, doi: 10.1007/s00190-017-1090-2

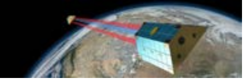

Literature (6)

Montenbruck, O., S. Hackel, M. Wermuth, F. Zangerl (2021): Sentinel-6A precise orbit determination using a combined GPS/Galileo receiver. Journal of Geodesy, 95, 109, doi: 10.1007/s00190-021-01563-z

Peter, H., U. Meyer, M. Lasser, A. Jäggi (2022): COST-G gravity field models for precise orbit determination of Low Earth Orbiting Satellites. Advances in Space Research, 69(12), 4155-4168, doi: 10.1016/j.asr.2022.04.005

Schaer, S., A. Villiger, D. Arnold, R. Dach, L. Prange, A. Jäggi (2021): The CODE ambiguity-fixed clock and phase bias analysis products: generation, properties, and performance. *Journal of Geodesy*, 95, 81, doi: 10.1007/s00190-021-01521-9

Schreiter, L., D. Arnold, V. Sterken, A. Jäggi (2019): Mitigation of ionospheric signatures in Swarm GPS gravity field estimation using weighting strategies. *Annales Geophysicae*, 37, 111-127, doi: 10.5194/angeo-37-111-2019

Svehla, D., M. Rothacher (2004): Kinematic Precise Orbit Determination for Gravity Field Determination, in *A Window on the Future of Geodesy*, edited by F. Sanso, pp. 181-188, Springer, doi: 10.1007/b139065

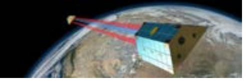

GNSS Background Literature

Teunissen, P.J.G., O. Montenbruck (2017): Springer Handbook of Global Navigation Satellite Systems, Springer, ISBN: 978-3-030-73172-4

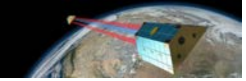

Kinematic LEO Orbit Products (1)

Arnold, D., A. Jäggi (2020): AIUB GRACE kinematic orbits, release 01. Published by Astronomical Institute, University of Bern. http://www.aiub.unibe.ch/download/LEO_ORBITS/GRACE, doi: 10.48350/158372.

Arnold, D., A. Jäggi (2020): AIUB GRACE-FO kinematic orbits, release 01. Published by Astronomical Institute, University of Bern. http://www.aiub.unibe.ch/download/LEO_ORBITS/GRACE-FO, doi: 10.7892/boris.147231.

Arnold, D., A. Jäggi (2020): AIUB Sentinel-1A kinematic orbits, release 01. Published by Astronomical Institute, University of Bern. http://www.aiub.unibe.ch/download/LEO_ORBITS/Sentinel-1A, doi: 10.7892/boris.145822.

Arnold, D., A. Jäggi (2020): AIUB Sentinel-1B kinematic orbits, release 01. Published by Astronomical Institute, University of Bern. http://www.aiub.unibe.ch/download/LEO_ORBITS/Sentinel-1B, doi: 10.7892/boris.145906.

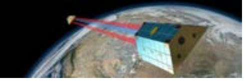

Kinematic LEO Orbit Products (2)

Arnold, D., A. Jäggi (2020): AIUB Sentinel-2A kinematic orbits, release 01. Published by Astronomical Institute, University of Bern. http://www.aiub.unibe.ch/download/LEO_ORBITS/Sentinel-2A, doi: 10.7892/boris.146129.

Arnold, D., A. Jäggi (2020): AIUB Sentinel-2B kinematic orbits, release 01. Published by Astronomical Institute, University of Bern. http://www.aiub.unibe.ch/download/LEO_ORBITS/Sentinel-2B, doi: 10.7892/boris.146133.

Arnold, D., A. Jäggi (2020): AIUB Sentinel-3A kinematic orbits, release 01. Published by Astronomical Institute, University of Bern. http://www.aiub.unibe.ch/download/LEO_ORBITS/Sentinel-3A, doi: 10.7892/boris.147286.

Arnold, D., A. Jäggi (2020): AIUB Sentinel-3A kinematic orbits, release 01. Published by Astronomical Institute, University of Bern. http://www.aiub.unibe.ch/download/LEO_ORBITS/Sentinel-3B, doi: 10.7892/boris.147287.

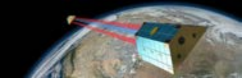

Kinematic LEO Orbit Products (3)

Arnold, D., A. Jäggi (2020): AIUB Swarm kinematic orbits, release 03. Published by Astronomical Institute, University of Bern. http://www.aiub.unibe.ch/download/LEO_ORBITS/SWARM, doi: 10.48350/158373.

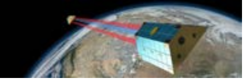

Pocket Guide of Least-Squares Adjustment (1)

The system of **Observation Equations** is given by:

$$\boldsymbol{L}' + \boldsymbol{\epsilon} = \boldsymbol{F}(\boldsymbol{X})$$

or, if $\boldsymbol{F}$ is a non-linear function of the parameters, in its **linearized** form:

$$\boldsymbol{L}' + \boldsymbol{\epsilon} = \boldsymbol{F}(\boldsymbol{X}_0) + \boldsymbol{A}\,\boldsymbol{x}$$

$\boldsymbol{L}'$	Tracking observations	$\boldsymbol{X}_0$	A priori parameter values
$\boldsymbol{\epsilon}$	Observation corrections	$\boldsymbol{x}$	Parameter corrections
$\boldsymbol{F}$	Functional model	$\boldsymbol{X}$	Improved parameter values, i.e., $\boldsymbol{X} = \boldsymbol{X}_0 + \boldsymbol{x}$
		$\boldsymbol{A} \doteq \left.\dfrac{\partial \boldsymbol{F}(\boldsymbol{X})}{\partial \boldsymbol{X}}\right\vert_{\boldsymbol{X}=\boldsymbol{X}_0}$	First design matrix

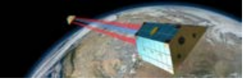

Pocket Guide of Least-Squares Adjustment (2)

The system of **Normal Equations** is obtained by minimizing $\boldsymbol{\epsilon}^T\, P\, \boldsymbol{\epsilon}$:

$$\left(\boldsymbol{A}^T\,\boldsymbol{P}\,\boldsymbol{A}\right)\,\boldsymbol{x} - \boldsymbol{A}^T\,\boldsymbol{P}\,\boldsymbol{l} = \boldsymbol{N}\,\boldsymbol{x} - \boldsymbol{b} = \boldsymbol{0}$$

$\boldsymbol{N} \doteq \boldsymbol{A}^T\,\boldsymbol{P}\,\boldsymbol{A}$	Normal equation matrix
$\boldsymbol{b} \doteq \boldsymbol{A}^T\,\boldsymbol{P}\,\boldsymbol{l}$	Right-hand side with "O-C" term $\boldsymbol{l} \doteq \boldsymbol{L}' - \boldsymbol{F}(\boldsymbol{X}_0)$
$\boldsymbol{P} = \sigma_0^2\,\boldsymbol{C}_{\boldsymbol{ll}}^{-1}$	Weight matrix, from covariance matrix $\boldsymbol{C}_{\boldsymbol{ll}}$ of observations

For a **regular** normal equation matrix the parameter corrections follow as:

$$\boldsymbol{x} = \left(\boldsymbol{A}^T\,\boldsymbol{P}\,\boldsymbol{A}\right)^{-1}\,\boldsymbol{A}^T\,\boldsymbol{P}\,\boldsymbol{l} = \boldsymbol{N}^{-1}\,\boldsymbol{b}$$

Pocket Guide of Least-Squares Adjustment (3)

The **a posteriori standard deviation of unit weight** is computed as:

$$m_0 = \sqrt{\frac{\boldsymbol{\epsilon}^T \, P \, \boldsymbol{\epsilon}}{f}}$$

f Degree of freedom (number of observations minus number of parameters)

The **covariance matrix** of the adjusted parameters is given by

$$\boldsymbol{C_{xx}} = m_0^2 \, \boldsymbol{Q_{xx}} = m_0^2 \, \boldsymbol{N}^{-1}$$

and their a posteriori standard deviations follow from the diagonal elements:

$$m_x = \sqrt{C_{xx}} = m_0 \, \sqrt{Q_{xx}}$$

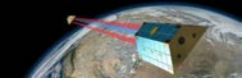

Pocket Guide of Least-Squares Adjustment (4)

Parameter pre-elimination is useful to handle a large number of parameters efficiently. Let us sub-divide the system of normal equations into two parts:

$$\begin{pmatrix} \boldsymbol{N}_{11} & \boldsymbol{N}_{12} \\ \boldsymbol{N}_{21} & \boldsymbol{N}_{22} \end{pmatrix} \cdot \begin{pmatrix} \boldsymbol{x}_1 \\ \boldsymbol{x}_2 \end{pmatrix} = \begin{pmatrix} \boldsymbol{b}_1 \\ \boldsymbol{b}_2 \end{pmatrix}$$

We we may reduce the normal equation system by pre-eliminating epoch-specific parameters $\boldsymbol{x}_2$, which yields the modified system of normal equations as

$$\boldsymbol{N}_{11}^{*}\, \boldsymbol{x}_1 = \boldsymbol{b}_1^{*}$$

where

$\boldsymbol{N}_{11}^{*} = \boldsymbol{N}_{11} - \boldsymbol{N}_{12}\, \boldsymbol{N}_{22}^{-1}\, \boldsymbol{N}_{21}$ is the normal equation matrix of $\boldsymbol{x}_1$

$\boldsymbol{b}_1^{*} = \boldsymbol{b}_1 - \boldsymbol{N}_{12}\, \boldsymbol{N}_{22}^{-1}\, \boldsymbol{b}_2$ is the corresponding right-hand side of the normal equation system

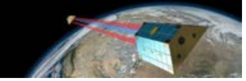

Main Results from Lab 2 (1)

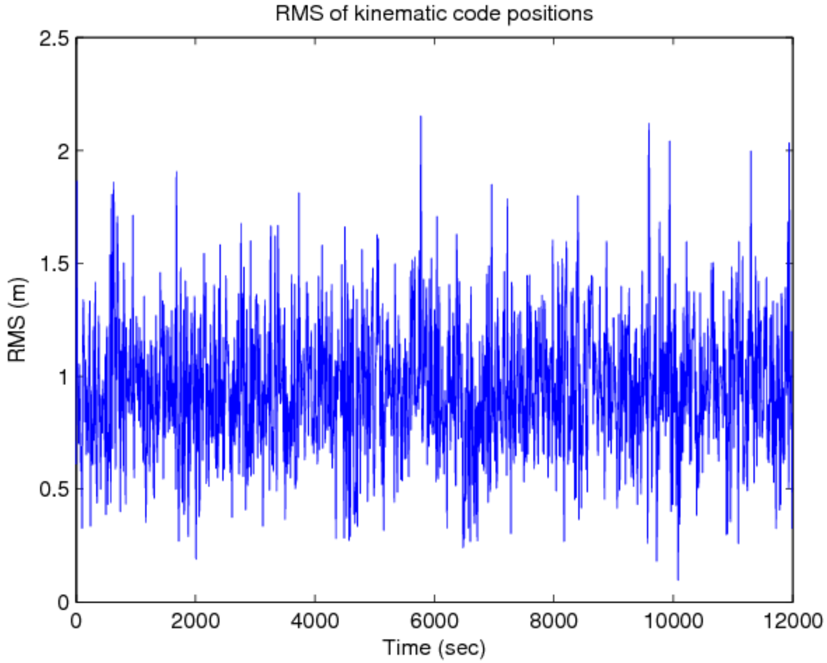

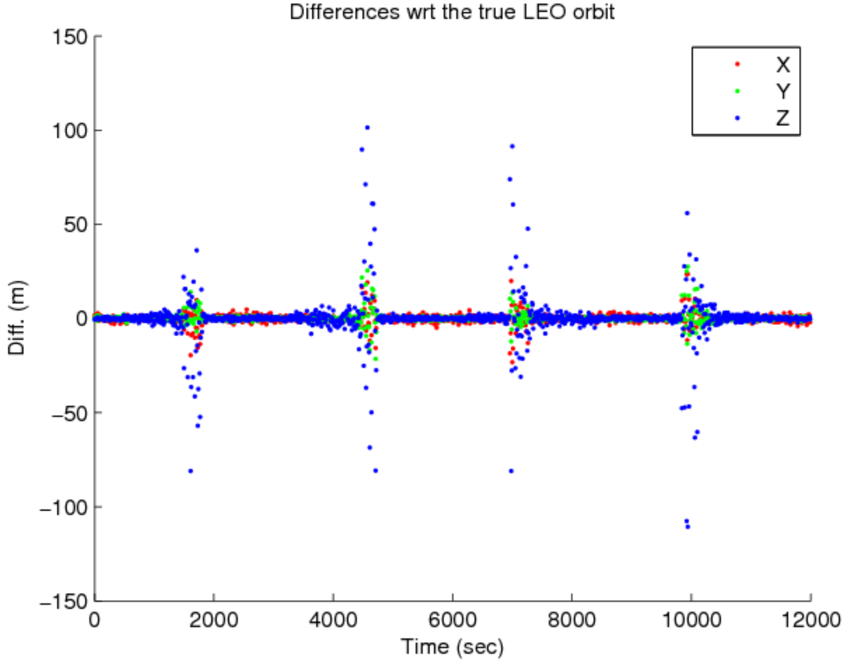

The **a posteriori RMS of unit weight** (m_0) of a Code-only kinematic LEO point positioning varies between about 0.5m and 2m (left).

The differences between the estimated kinematic positions and the true LEO orbit show large deviations twice-per-revolution (right).

Main Results from Lab 2 (2)

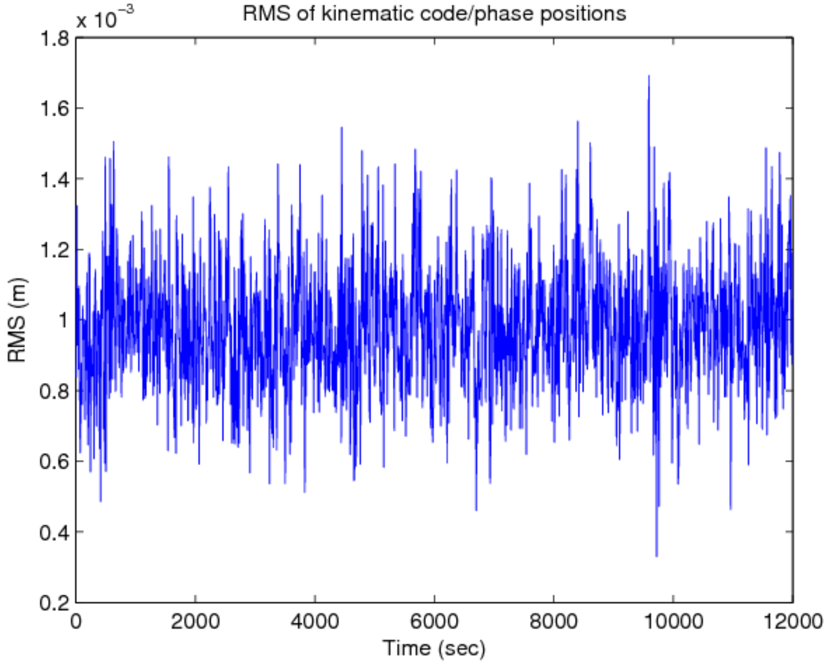

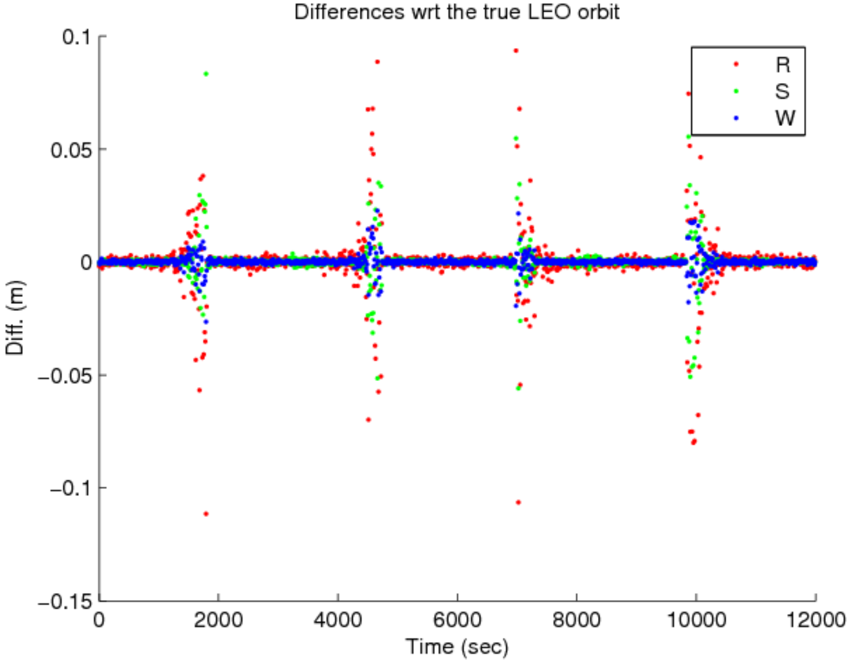

The **a posteriori RMS of unit weight** (m_0) of a combined Code- and Phase kinematic LEO point positioning varies between about 0.6 and 1.4mm (left).

Due to the phase observations the quality of the kinematic positions has reached **sub-cm accuracies** for most epochs. Problematic phases twice-per-revolution, however, are still visible.